Evaluating spatial and temporal variations in sub-field level crop water demands

by

Travis Wiederstein

B.S., Kansas State University, 2021
M.S., Kansas State University, 2021

A THESIS

submitted in partial fulfillment of the requirements for the degree

MASTER OF SCIENCE

Carl and Melinda Helwig Department of Biological and Agricultural Engineering
Carl R. Ice College of Engineering

KANSAS STATE UNIVERSITY
Manhattan, Kansas

2021

Approved by:
Co-Major Professor
Dr. Jonathan Aguilar

Approved by:
Co-Major Professor
Dr. Vaishali Sharda

Copyright

Abstract

Existing Variable Rate Irrigation (VRI) practices use soil electrical conductivity, historical yields, and topographic maps to delineate variable rate zones. However, these methods are not conducive to tracking within season variability in crop water demands. With increasing remote sensing data availability, in-season maps of crop coefficients and evapotranspiration (ET) may help inform variable rate irrigation schedules. Although, the amount of spatial and temporal variation in crop coefficients at the sub-field level has not been widely researched. This study aims to compare subfield ET estimates from two remote sensing platforms and quantify spatial and temporal variations in sub-field level ET. Vegetation indices and reference ET data were collected at Kansas State University's Southwest Research Extension Center (SWREC) and two Water Technology Farms during the 2020 corn growing season. Weekly maps of the normalized difference vegetation index (NDVI) and the soil-adjusted vegetation index (SAVI) from manned aerial imagery were combined with empirical equations to estimate both basal and combined crop coefficients at a 1-meter resolution. These coefficients were combined with local reference ET estimates, aggregated to a 30-meter resolution, and compared to the Landsat Provisional Actual Evapotranspiration dataset. Finally, actual ET estimates from aerial images were aggregated using K-means clustering and stationary variable speed zones to determine if there is enough variation in actual ET at the sub-field level to build variable rate irrigation schedules. An equivalence test demonstrated that the aerial imagery and Landsat data sources produce significantly different crop coefficient estimates. However, the two datasets were moderately correlated with Pearson's product-moment correlation coefficients ranging from -0.95 at the SWREC to 0.63 and 0.86 at the two Water Technology Farms. Both the aerial imaging and Landsat datasets showed high variability in crop coefficients during the first 5-6 weeks after emergence, with these coefficients

becoming more spatially uniform later in the growing season. These crop coefficients may help irrigators make more informed irrigation management decisions during the growing season. However, more research is needed to validate these remotely sensed ET estimates and integrate them into an irrigation decision support system.

Table of Contents

List of Figures

List of Tables

Acknowledgements

First and foremost, I would like to thank my supervisory committee for their guidance throughout this research. I would especially like to thank my advisor, Dr. Vaishali Sharda, for her honest feedback, patience, and advice over the last two years. I would also like to thank Dr. Stacy Hutchinson for her encouragement to pursue graduate school, and her advice during my time as an undergraduate student at Kansas State University.

This work could not have been completed without the help of Kansas State University's Southwest Research Extension Staff, especially Dr. Jonathan Aguilar, Bruce Niere, Jake Thompson, and Dennis Tomsicek. Dr. Jonathan Aguilar also served as my co-major advisor and helped make my time in Garden City, KS incredibly memorable. Thank you all for your hard work and support during the 2020 growing season. I would also like to thank the KSU NRT faculty, our data providers, and Sarah Bratschun, for technical assistance and professional growth opportunities throughout this project. The satellite imagery used in this research was collected and distributed by the U.S. Geological Survey, and this work was funded by the National Science Foundation Grant #1828571.

I cannot thank all my friends and family enough for their support throughout my college career. I especially want to thank my parents, Karen and Bob Wiederstein, as well as my in-laws, Karen and Jerry Ripperger for their unwavering love and support throughout this journey. I also owe a huge thank you to Dawson and Aubrey Borcherding for providing me with a place to stay at the last minute during my thesis defense. You are two of the most Christ-like people I know, and I am incredibly thankful for your friendship. Lastly, I am eternally grateful for my wife, Sarah, and her endless patience, love, and support over the last three years. There were dozens of times when I wanted to quit, but you helped keep me grounded through the storm.

Chapter 2 - Introduction

1.1 Problem Statement

Water levels in the Central and Southern Regions of the High Plains Aquifer (HPA) have decreased since the 1950s (McGuire, 2017). Two main contributors to these declines are the invention and widespread adoption of center pivot irrigation, and the over-appropriation of water rights during the first few decades after the Kansas Water Appropriation Act was passed in 1945 (Sheffield, 1970; Sophocleous, 2012). These two factors allowed farmers to plant more water intensive crops, like corn and alfalfa, in areas that are not naturally suited for their growth (Perry, 2006). Now, both employment rates and gross domestic product in Kansas are heavily dependent on irrigation water from the High Plains Aquifer (Tidwell et al., 2016). However, if the current depletion rates continue, many parts of the HPA will not be able to support irrigation by 2042 (Scanlon et al., 2012). Additionally, the path to sustainable groundwater use in the HPA is not straightforward. Researchers, community members, and policy makers have all proposed different strategies to reduce groundwater pumping. These propositions are further discussed in section 2.6.

Regardless of the path to sustainability, many irrigators will need to change their management practices to maintain high yields under decreased water availability. This is especially true under existing long-term climate change and population growth projections (Cotterman et al., 2018; Elliott et al., 2014; Marshall et al., 2015; Wada et al., 2013). Higher atmospheric temperatures and both spatial and temporal changes to rainfall patterns will likely result in less rainfall during the existing growing season (Harding & Snyder, 2012). Meanwhile, the global population is expected to reach over 9 billion by 2050 (Godfray et al., 2010), which will increase crop demands by up to 100% relative to 2005 (Tilman et al., 2011). In the absence of any large-scale mitigation strategies, the total area used for irrigated agriculture and total corn production in

the HPA are expected to decrease by 60% and 20-30% by the end of this century, respectively (Cotterman et al., 2018). All these changes contribute to decreased stability in the HPA region, and will force irrigators to adapt using new irrigation strategies.

Two strategies that can improve water use efficiency are deficit and Variable Rate Irrigation (VRI) (Ajaz et al., 2020; Evans & King, 2012; O'Shaughnessy et al., 2016). Deficit irrigation only schedules irrigation often enough to keep soil water availability above an allowable depletion level. This allows crops to experience some level of water stress during non-critical growth stages with negligible impacts on crop yields (Land and Water Division, 2002). Variable rate irrigation applies different amounts of water to different parts of a field based on knowledge of sub-field level crop water demands. Both deficit and VRI require high spatial and temporal resolution input to correlate with crop water demands. Existing decision support systems for these irrigation methods use intrusive data sources that often only capture data at a single, or at best a few, points within a field to monitor crop water demands. New decision support systems may benefit from high resolution remote sensing data (Zhang et al., 2021). Based on this fact, this study attempts to evaluate new data sources to help inform deficit and variable rate irrigation decisions.

1.2 Objectives

This study was undertaken to conduct a comparison of remotely sensed crop coefficients and actual ET estimates using two different platforms: Landsat 8's Provisional Actual Evapotranspiration data set and aircraft-based multispectral imagery. While each platform uses similar data (i.e., multispectral images) to estimate spatial patterns of actual ET and crop coefficients, each platform has its own processes for atmospheric correction and the conversion of reflectance measurements to actual crop ET. Each platform also measures a slightly different range of the electromagnetic spectrum, and each platform has its own practical limitations to its

usefulness in informing in-season management decisions. The purpose of this study is to: 1) compare crop water demands at the sub-field level using two new data sources, and 2) evaluate the spatial and temporal variability in sub-field level crop water demands.

Chapter 3 - Literature Review

2.1 Foreword

The High Plains Aquifer supplies between 70 and 80% of all water used in Kansas. This high dependence on groundwater, especially in Western Kansas, has led to unsustainable depletion rates and several water-related issues (Buchanan et al., 2001). These issues have led to the creation of several state agencies, research initiatives, and grassroots community organizations to help protect this natural resource. Many researchers, notably Elshall et al. (2020), Sanderson & Frey (2015), Smidt et al. (2016), and Sophocleous, (2012), have provided a more in-depth overview of the political and cultural evolution related to groundwater use in Kansas. The following literature review summarizes the invention of center pivot irrigation, the expansion of irrigated agriculture in the HPA, key policies that have tried, and at times, failed to protect groundwater sustainability in the HPA, and current recommendations to reach sustainability in the HPA. This literature review appropriately frames the remaining chapters of this thesis as a small step towards increasing irrigator's ability to make more informed management decisions.

2.2 Invention of Center Pivot Irrigation and Groundwater Depletion in the High Plains Aquifer

Few inventions have changed the shape of agriculture more than the center pivot irrigation system. In 1952, Mr. Frank Zybach was issued a patent for this system, which used a pipe with nozzles installed along it to irrigate large areas as it pivoted around a central point in a field. The rights to the patent were later sold to Valley Manufacturing Company (now Valmont Industries). Soon after, center pivot systems were widely sought to help farmers maintain high yields during seasons of drought, which hit in the 1950s. The Dust Bowl, which began less than two decades

before the center pivot's invention, made farmers more open to adopting new technologies to combat droughts. These memories, combined with Valley Manufacturing Company's ability to efficiently build and market this system, led to the expansion of irrigated agriculture. This expansion was also aided by center pivot irrigation's ability to address many of the shortfalls of existing irrigation practices, like flood and furrow irrigation (Sheffield, 1970). These irrigation practices could not be used in areas with rough topography and sandy soils because they drastically increase soil erosion. While the introduction of the center pivot simplified irrigation operations and reduced excess water use compared to existing irrigation techniques, their widespread use only temporarily stopped water availability issues in many regions. Instead, center pivot systems allowed farmers to grow crops with higher water demands (i.e., alfalfa and corn) in climates that are not naturally suited for their cultivation (Perry, 2006). In the short term, this increased agricultural production led to major economic growth in rural regions. In the long term, this positive feedback loop between crop availability and economic growth has led to unstable groundwater withdrawals in some regions, including most of the Central and Southern portions of the High Plains Aquifer (HPA). Figure 1 below from McGuire (2017) shows the change in aquifer water levels across the entire HPA, from predevelopment to 2015. If depletion continues at this rate, up to 35% of the Southern HPA will be unable to support irrigation by the year 2042 (Scanlon et al., 2012).

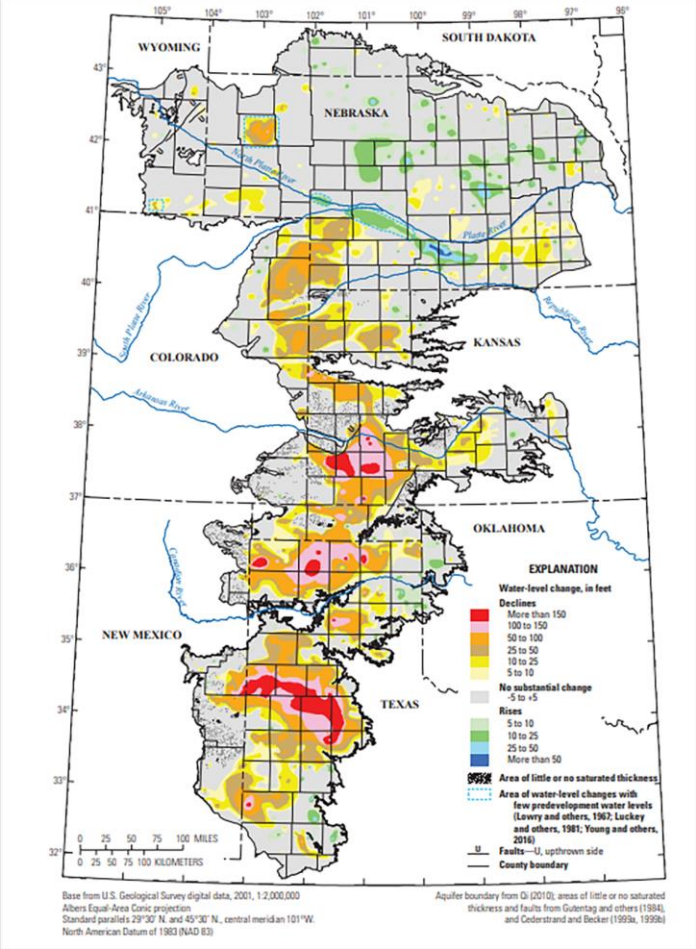

Figure 1. Changes in aquifer depth from predevelopment to 2015. Developed by McGuire (2017)

2.3 Improved Center Pivot Irrigation Efficiency

Since their invention and widespread adoption, many upgrades to center pivot systems have continued to improve their water and energy efficiencies. Among these technologies are new hydraulic, electric, and pneumatic drive systems, more efficient pumps, new types of nozzles, and automated control systems. Irrigators can choose from thousands of center pivot configurations, and work with irrigation equipment manufacturers to meet their specific needs. However, improvements to the center pivot system have failed to reduce groundwater pumping. Instead,

irrigators often expand their irrigated acreage when they improve their irrigation efficiency. This phenomenon of expanded groundwater use with the adoption of more efficient irrigation technology is referred to as Jevin's Paradox, and it is primarily driven by well-intentioned policies and a false sense of security that comes with new technology (Pfeiffer & Lin, 2010, 2014; Sears et al., 2018). One specific example of Jevin's Paradox is the increase in drop-nozzle use on center pivots in all five of Kansas' GMDs between 1991 and 2003. This new technology improved irrigation efficiency by reducing wind drift, and its adoption was aided by government subsidies. During the same period, groundwater withdraws showed no statistically significant change despite this improved efficiency (Perry, 2006). On one hand, this means that irrigators were able to produce more crops with the same amount of water. However, this improved efficiency did not lead to reduced pumping, or extend the useful life of the Central and Southern High Plains Aquifer. Unfortunately, this is only one example of a well-intentioned policy that has proved to be ineffective at reducing groundwater withdrawal in the High Plains. Part of this policy failure is often blamed on a lack of consideration for irrigator responses. This disconnect between government agencies and community members has caused a rift in how water conservation is managed, and further complicated the water management structure in Kansas (Sanderson & Frey, 2015).

2.4 Brief History of Groundwater Management Policies in Kansas

Sophocleous (2012) provides a well-rounded history of the agencies and policies that have shaped Kansas' water management structure into its current state. Most notable amongst these are the Kansas Water Appropriation Act (KWAA) of 1945 and the Groundwater Management District Act (GMDA) in 1972. Arguably, most of Kansas' water problems originate back to a lack of

oversight in the initial implementation of the KWAA. The KWAA allowed irrigators operating before 1945 to continue normal operations, while new irrigators were required to file an application before withdrawing from the High Plains Aquifer. The original permitting program was not well regulated, and a lack of application scrutiny led to overdevelopment in the HPA, especially in Western Kansas. However, the impact of increased development was not uniform across the entire state because saturated groundwater thicknesses, annual rainfall, and aquifer recharge rates vary regionally. Recognizing this, legislators created five Groundwater Management Districts in the 1970s to advise the Chief Engineer of the Division of Water Resources regarding water conservation plans and policies throughout the state. Since then, several revisions to the KWAA and GMDA have changed how much water irrigators can withdraw in each GMD. These withdrawal rates are based on each GMD's goals and range from a "safe-yield" approach, which balances withdraws with recharge, to a "planned depletion" approach, which treats groundwater as a nonrenewable resource, but allows a given amount of depletion over a given timespan (Sophocleous, 2012). Additional revisions have changed the actual amount of depletion in each district because the amount of recharge in most districts was originally overestimated. While many of the oversights in the water permitting process have since been fixed, much of the damage, especially the over development of Western Kansas, is difficult to undo. Currently, there are three primary ways to directly reduce the amount of irrigated land in Kansas. The first requires the Chief Engineer to leverage the 1978 GMD Act revision that allows for the designation of an Intensive Groundwater Use Control Area (IGUCA). The IGUCA clause is currently the only explicit means for the government to restrict existing water rights. However, this "top-down" approach poses some legal and political risks on the Chief Engineer and is generally not supported by producers (Griggs, 2014; Golden and Leatherman, 2019). The second is the creation of Local Enhanced

Management Areas (LEMAs). This program was introduced into Kansas' water laws in 2012 and follows a producer-led "bottom-up" approach where irrigators from a contiguous area conduct a hearing to develop a conservation plan. Once this plan is approved by the Chief Engineer, it becomes law. It should be noted that a conservation plan in a LEMA does not have to explicitly reduce irrigated acreage. Results from the Sheridan #6 LEMA show that reducing irrigated acreage was one strategy used by members of the LEMA (Golden, 2016), although other water use reduction methods had greater impacts (Drysdale & Hendricks, 2018). The third way to reduce irrigated acreage is through voluntary farmer enrollment in the Conservation Reserve Enhancement Program (CREP). If accepted for this program, farmers are paid a fixed rate to remove a portion of their land from development. Typically, this land must be taken out of rotation for 10-15 years to receive benefits, and there are caps on the maximum amount of land per county that can be enrolled.

Despite these programs, depletion of the High Plains aquifer has continued. Sanderson & Frey (2015) attempt to explain this lack of progress as a mismatch between the scale of the existing proposed solutions and the scale of resource exchange. More specifically, these authors explain that groundwater depletion should not be defined by the physical boundaries of the aquifer. Instead, groundwater depletion is the result of exchanges at the global scale because water from the HPA helps produce food for people around the world—not just locally. However, the consumers of these goods do not bear the long-term cost of water depletion. When the HPA is exhausted, the communities geographically located in and around the HPA will bear most of the financial hardship. In contrast, those consuming the food grown and produced in the HPA will have their needs met from other sources.

2.5 Other Barriers to Reducing Groundwater Depletion in the HPA

Several other challenges have complicated groundwater issues in the HPA region including climate change, poor modeling assumptions, and a lack of communication between irrigators, researchers, and legislators. Climate change projections show a likely increase in temperatures and more frequent prolonged droughts that will increase crop water demands (Harding & Snyder, 2012). While there is uncertainty in climate change projections, modeled scenarios show up to a 65% decrease in irrigated corn yields, and a 20-30% decrease in total corn yields by the end of this century (Cotterman et al., 2018). Inaccurate assumptions in groundwater models may be discouraging irrigators and policy makers from enacting changes (Butler et al., 2020). These researchers specifically cite high uncertainty and improper calibration methods in modeled scenarios, which lead to inappropriate specific yield values and overestimations of pumping reductions required to reach sustainable withdrawal. Finally, many irrigators believe that they personally have little ability to decrease water use on their own farms, primarily due to a lack of time (Lauer & Sanderson, 2020), and a lack of unbiased information surrounding the best water conservation practices (Lamm & Porter, 2017). These barriers have resulted in declining attendance rates at outreach events designed to demonstrate new technologies and foster discussion around water conservation (Porter et al., 2020).

2.6 Proposed paths to Reaching Sustainability in the HPA

To address the mismatch between the scale of the existing solutions and the scale of resource exchange, Sanderson and Frey (2015) suggest that groundwater depletion must be addressed by adjusting product pricing to reflect the cost of its environmental impacts and placing a cap on irrigators' water footprints. However, this full-cost pricing would need to be implemented

on an international scale to prevent competition between, and further exhaust resources in, other countries. Additionally, the cap on irrigators' water footprints would address Jevin's Paradox by limiting the amount that producers can expand their irrigated land as their profits increase. Addressing climate change will require a combination of several strategies to offset rising temperatures and increased crop water demands. Examples of these strategies include changing planting dates, transitioning to more drought-tolerant crops, installing more efficient irrigation technology, and adopting deficit irrigation, or other irrigation scheduling techniques that only apply irrigation when absolutely necessary (Ajaz et al., 2020; Basso et al., 2013; Lobell & Burke, 2010). New analyses are placing the groundwater depletion in context of Western Kansas' food-energy-water nexus to understand what drives stakeholder participation in conservation programs. These analyses identify a need for policy makers and research extension specialists to prioritize farmers' profits, incorporate both short- and long-term goals into decisions, reduce operation risks, increase the political desire to conserve groundwater, and provide on-demand resources regarding best management practices. More broadly speaking, placing groundwater withdrawals in the greater context of the food-energy-water nexus allows stakeholders to understand how this problem evolved to its current state and what social and political elements of the system could be addressed to better promote sustainable groundwater use.

2.7 Introduction to Advanced Irrigation Scheduling Techniques

From the aforementioned literature, it is clear that new technology alone is not the solution to reaching sustainable water use in the High Plains Aquifer. Rather, a combination of political and social reform, market adjustments, and new technologies must be used to extend the useful life of the High Plains Aquifer, while promoting the economic well-being of rural communities and

meeting future food demands (Smidt et al., 2016). Therefore, researchers must continue to identify effective and efficient management techniques, so irrigators have options when water availability becomes scarce, or new policies restrict its use. Advanced irrigation scheduling techniques, like deficit and variable rate irrigation may help irrigators maintain high yields in a water-limited future (Ajaz et al., 2020).

Deficit irrigation schedules irrigation events once, or right before, soil moisture contents reach a critical threshold. This method can prevent overwatering by allowing some amount of soil moisture depletion without negatively impacting yields or producers' profits. A review by (Rudnick et al., 2019) summarized the methods and results of several deficit irrigation projects in Kansas, Texas, Nebraska, and Colorado. The authors identified varying motivations for switching to deficit irrigation, including decreased water availability, new state policies dictating water use, and soil and climate factors, like rainfall distribution. The authors also identified a few strategies that were effective at nearly all locations, including: 1) adjusting deficit irrigation schedules based on site-specific conditions, 2) changing deficit irrigation scheduling based on crop growth stages to avoid water stress during critical growth stages, and 3) combining deficit irrigation with other conservation practices, like reduced tilling.

While many deficit irrigation strategies vary irrigation depths throughout the growing season to account for temporal changes to crop water demands, they typically do not account for spatial changes in crop water demands. Under both deficit and non-deficit irrigation scheduling, producers typically apply a uniform amount of water to an entire field. However, actual crop demands can vary through space and time (spatiotemporally) based on plant density, growth stage, plant health, topography, soil properties, crop genetics, and the presence of pests or diseases, among many other factors (Evans & King, 2012). To meet these variable demands, researchers and agricultural

technology companies have developed speed and flow rate control systems for center pivots. For further details about the early design and function of these systems, see (Ian R. McCann & Jeffery C. Stark, 1991; M. Omary et al., 1997). A review by (W. L. Kranz et al., 2012) describes many of the control mechanisms, sensor types, and communication protocols created to control these systems. At the time of its publication, the review identified a need to focus on commercial development of decision support systems to help automate the irrigation prescription process.

Since 2012, there has been a large surge in the number of decision support systems available for irrigators to automate their VRI systems. Many of these decision support systems use physical soil properties, historical yield data, and *in situ* sensors to estimate crop water demand at subfield scales. While networks of soil sensors have been used for VRI scheduling, many common soil moisture sensors do not have the required level of accuracy and sensitivity needed for VRI, and they can be intrusive to normal operations (Evett et al., 2014). Instead, many decision support systems delineate management zones using maps of field topography, soil electrical conductivity, and historic yields (Lo et al., 2017; Svedin et al., 2021). However, these maps only account for the spatial variability in site specific properties that contribute to differences in crop water demand. These maps do not provide in-season irrigation prescriptions based on actual crop water demands. To account for this, researchers have combined these maps with thermal sensors and local weather data to monitor crop water stress (Blonquist Jr. et al., 2005; Casanova et al., 2012; Evett et al., 2009; Mahan et al., 2010; O'Shaughnessy & Evett, 2008; S. A. O'Shaughnessy & S. R. Evett, 2010). This data is typically used to calculate water stress indices, which are compared to critical values to determine when, and how much irrigation to apply. Two common methods are time temperature threshold (TTT) and crop water stress index (CWSI) monitoring. TTT scheduling is based on the concept that plants are most productive under a narrow range of temperatures, called

the thermal kinetic window (Burke, 1993). Under this scheduling method, sensors monitor crop canopy temperatures and a decision support system triggers irrigation if the temperature exceeds a given threshold for an extended period. (Evett et al., 2002) recommends triggering irrigation once corn is above 28°C for 240 minutes in the Central and Southern High Plains Region. In contrast, the CWSI uses a combination of canopy and air temperatures to determine crop water stress. In this method, the difference between the air and canopy temperatures are compared to reference temperature differences for dry, bare soil and full developed, non-water stressed canopies. This framework, developed by Jackson et al. (1981), greatly simplified earlier energy balance approaches used to determine crop water stress. Several researchers have integrated the CWSI into irrigation schedules with mixed success. Gu et al. (2020) provides an overview of these different methods, and challenges related to the use of the CWSI. Most notably, the need for accurate estimates of minimum and maximum temperature differences has limited the widespread use of the CWSI. To account for variability in these temperature differences throughout the growing season, Moran et al. (1994) developed the Water Deficit Index (WDI). The WDI uses the CWSI in combination with a vegetation index, like the normalized deficit vegetation index (NDVI), to create dynamic reference temperatures that vary based on the level canopy cover. Graphically, they present their results as the vegetation index/temperature (VIT) trapezoid, shown in Figure 2.

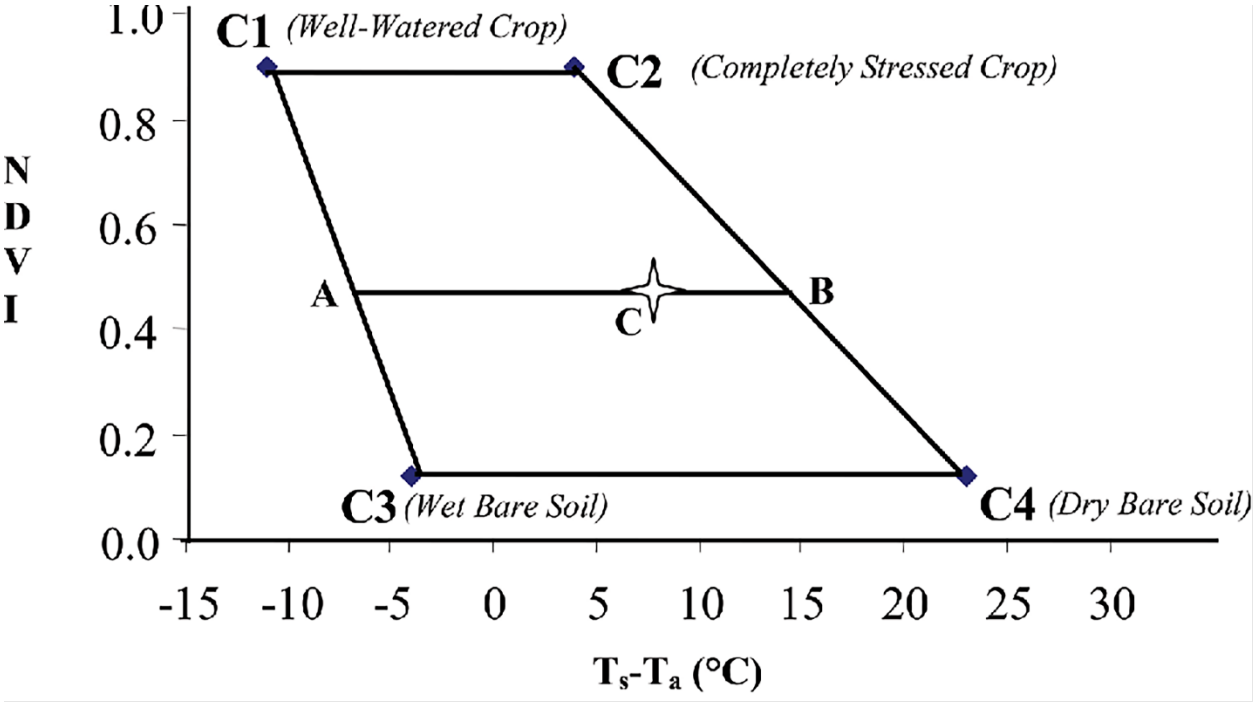

Figure 2. Visualization of the Vegetation Index/Temperature Trapezoid. From Colaizzi et al. (2000)

Multiple decision support systems are available to integrate all these indices into the VRI scheduling process (Andrade et al., 2020; Evett et al., 2020; Liakos et al., 2015; Shi et al., 2019; Stone et al., 2020). One of the most advanced systems, ISSCADA is presented by (Andrade et al., 2020), evaluated for humid regions by Sui et al. (2020), and patented by Evett et al. (2014). However, this system primarily uses stationery and pivot-mounted sensors, which only provide partial measurements of canopy temperatures and soil water content across a field at any given moment. Alternatively, (Serrano et al., 2020) used satellite NDVI images to account for changing crop growth stages across an entire field in a VRI decisions support system.

2.8 Gaps in Variable Rate Irrigation Scheduling

While the introduction and integration of these new indices has advanced the practicality of VRI, most VRI decision support systems are still incapable of providing support based on both

high spatial and temporal resolution estimates of crop water demands. Additionally, decision support systems based on water stress indices typically require knowledge of local, experimentally determined critical stress thresholds, like those needed for CWSI approaches.

In contrast, data for traditional evapotranspiration-based irrigation scheduling is often readily available from national-, state-, or university-funded sensor networks, like the Kansas Mesonet. The Kansas Mesonet is a network of over 60 weather stations that estimates reference evapotranspiration (ET) values across the state of Kansas. For irrigation management decisions, evapotranspiration from a reference crop (ET_0) must be converted to actual evapotranspiration using a crop coefficient. Multiple methods exist to convert ET_0 values to actual crop ET, including the use of single and dual crop coefficients. Doorenbos and Pruitt (1977) proposed the single crop coefficient method, which uses a single coefficient to estimate soil evapotranspiration and crop transpiration when combined with ET_0. Alternatively, Allen et al. (2005) presented a dual coefficient approach, which splits the single crop coefficient into two components to account for soil evaporation separately from plant transpiration. Both the single and dual crop coefficient approaches depend on a crop's growth stage. However, growth stages for these coefficients are typically only divided between early, mid, and late season, and do not reflect daily changes in crop water demands based on in-field measurements. Several authors contributed early, mid, and late season crop coefficients for several common crops, including Doorenbos and Kassam (1979), Doorenbos and Pruitt (1977), Pruitt (1986), Wright (1981, 1982), and Snyder et al. (1989). Other researchers have developed mathematical models to calculate crop coefficients using growing degree days (GDD) (Sammis et al., 1985). While both these approaches use time since planting to determine crop coefficients, they do not use live measurements of crop growth stages to determine the appropriate crop coefficient. Additionally, neither the growth stage nor the GDD methods

account for spatial variability in crop growth stages that result from variable soil, topographic, and environmental factors. Rather, they are commonly used to calculate a single crop coefficient for an entire field. While both single and dual crop coefficients are useful for irrigation scheduling, neither has been widely used for variable rate irrigation due to a lack of knowledge of the crop growth stages and soil water availability at the subfield level.

2.9 Remote Sensing in Agriculture

New sources of remote sensing information may be useful for identifying high spatial and temporal differences in crop water demands (Calera et al., 2017). Remote sensing, especially satellite imagery, is often used to study changes in vegetation properties, including crop coefficients, at national, regional, and field scales (Zhang et al., 2016). Satellite platforms are especially useful for monitoring crop water demands in data-sparce areas (Sheffield et al., 2018). However, satellite images are not always available at the right time, or the right spatial resolution to be useful for agricultural management (Rudd et al., 2017). Additionally, further validation and processing frameworks are needed to make satellite images useful for irrigation management (Blatchford et al., 2019; Karthikeyan et al., 2020; Sishodia et al., 2020; Talsma et al., 2018). In contrast, drones have been used as a remote sensing platform in agriculture for plant emergence monitoring, weed detection, crop damage or illness mapping, and crop water stress mapping to detect equipment malfunctions (Daponte et al., 2019; Maes & Steppe, 2019; Mukherjee et al., 2019; van der Merwe et al., 2020). However, these authors recognize that collecting and processing drone data can be very time-consuming and labor-intensive. Multispectral cameras mounted to small commercial aircraft can collect similar data at a 1-meter spatial resolution, and a temporal resolution of up to a week, which may provide an ideal compromise between consistency of satellite imagery and the high spatial resolution of drone imagery. However, data from these three

sources have not been used to determine if there are high enough spatial and temporal differences in crop coefficients to inform VRI schedules.

In the 1980s, researchers began developing methods to predict crop growth stages and actual evapotranspiration from remote sensing platforms (Glenn et al., 2011; Pinter, Jr. et al., 2003). Critical to this research was the development of multispectral indices, simple ratios of reflectance values in different parts of the electromagnetic spectrum (Glenn et al., 2011; Pinter, Jr. et al., 2003). Two indices commonly used for crop monitoring are the normalized difference vegetative index (NDVI) created by Rouse et al. and the soil adjusted vegetation index (SAVI) created by Huete, which are calculated using red and NIR light (Huete, 1988; Rouse et al., 1974). Using maps of reflectance indices has since become a simple and popular way to monitor spatial distributions of crop growth ET at large spatial scales. Pôças et al. (2020) provides a review of techniques and best practices for converting multispectral imagery to single and basal crop coefficients for. Their review includes regression equations from existing literature that estimate crop coefficients from NDVI and SAVI. More details regarding each equation's development are presented in the following paragraphs.

Bausch & Neale (1987) developed reflectance-based crop coefficient curves using daily measurements of basal crop coefficients and NDVI. This research was conducted at a research plot in Greeley, CO. The researchers used a hand-held radiometer to measure red and near-infrared reflectance values 2 meters above the crop canopy near solar noon and related these measurements to crop coefficients calculated using knowledge of planting dates and crop growth stages.

This work was later expanded by Neale et al. (1989), who used more detailed estimates of the basal crop coefficient. The basal crop coefficient was calculated as the fraction of ET of corn to the ET of alfalfa, where the ET of corn and alfalfa were computed from a water balance equation

and weighing lysimeter data. This data was collected at the original Greeley, CO location, as well as an additional research site near Fruita, CO. The linear equation between the basal crop coefficients and NDVI was based on those values measured for bare soils and fully developed cover. The reflectance-based crop coefficient curve was developed using a Richards growth curve function. The actual basal crop coefficients were within -2.6% and 4.7% of the reflectance-based coefficients.

(Bausch, 1993) recognized that these early equations were sensitive to soil background effects and could overestimate crop coefficients when used in areas with dark-colored soils. These researchers proposed a new linear model to relate basal crop coefficients to the Soil Adjusted Vegetation Index (SAVI). This index is similar to NDVI but includes a multiplication factor to account for soil noise under a range of canopy coverages. Results showed that this model was less sensitive to soil color, predicting basal crop coefficients that differed by less than 6% between dry, light color soils, and wet, dark colored soils.

Building off this work, (Campos et al., 2017) developed a linear model to calculate basal crop coefficients for irrigated and rainfed maize and soybeans using SAVI. In contrast to Bausch (1993), this research used data from Ameriflux towers near Mead, NE, and used SAVI measurements from the Landsat 5 and Landsat 7 satellites to predict the basal crop coefficient. The linear model was developed by relating SAVI to the basal crop coefficient under bare soil and full canopy conditions. This research showed strong agreement between the measured and predicted basal crop coefficients with RMSEs of 0.075 and 0.068 for maize and soybeans, respectively.

(Kamble et al., 2013) related MODIS satellite NDVI estimates to the combined crop coefficients, which were back-calculated using the FAO-56 dual crop coefficient method. The researchers attempted to build a robust crop coefficient-NDVI linear equation by combining three

data sets from different locations. Each location had a unique climate, soil classification, and crop rotation. The data sets used for model fitting included measurements from corn and soybean operations near Mead and Clay Center, NE and grasslands near Cottonwood, SD. The researchers used ET measurements from the Ameriflux tower network during 2006 and 2007. Their results showed a strong linear association between the back-calculated combined crop coefficient and MODIS NDVI measurements (r^2=0.9-0.91, and RMSE 0.16-0.19).

Finally, Senay (2018) and Senay et al. (2013) developed a method to compute fractional evapotranspiration using psychrometrics called the Operational Simplified Surface Energy Balance (SSEBop) model. In psychrometrics, humidity and vapor pressure can be calculated from the difference between dry-bulb and wet-bulb temperatures. The wet-bulb temperature is always lower than the dry-bulb temperature due to the cooling effect of evaporation. Generally, the higher the temperature difference between the two bulbs, the greater the evaporation rate. Senay (2018) and Senay et al. (2013) demonstrates that relative hot and cold satellite imagery pixels can represent these wet- and dry-bulb temperatures. When combined with a vegetation index, like NDVI, researchers can estimate the evapotranspiration rates for every pixel in a scene. Senay (2018) demonstrated relatively good agreement between these ET estimates and Ameriflux towers across the Contiguous United States, with an r^2 of 0.61. The USGS used these methods to develop the Landsat Provisional ET dataset. This dataset includes fractional ET datasets, which can be combined with local ET reference data to compute actual ET at a 30-meter resolution.

Despite these advancements in remote sensing technology for monitoring high resolution crop water demands, these technologies have not been widely adopted by irrigators. This may be due to several well-documented gaps in research around remotely sensed predictions of crop water demands, including: 1) uncertainty in the accuracy of the predictions, 2) a lack of frameworks to

efficiently convert remote sensing data into practical management decisions, and 3) a lack of research that quantifies improvements to irrigation efficiency resulting from schedules developed using remote sensing data. This research attempts to help bridge these gaps in existing literature by conducting on-site investigations into sub-field level crop water demands. These three gaps are not addressed entirely in this research, but this work helps pave the way for future researchers to develop new frameworks for data processing and quantify the impacts on irrigation operations resulting from remote sensing-based decisions. The following chapter details the steps taken to improve our understanding of sub-field evapotranspiration estimates from two remote sensing platforms.

Chapter 4 - Methods and Data Description

3.1 Site Descriptions

All data were collected on irrigated corn fields during the 2020 growing season. These fields are shown in Figure 1 below. The two quarter circle plots (Figure 3 (a) and (b)) are located on producer-owned fields and are part of Kansas Water Office's Water Technology Farm program. Field A is located approximately 17 km Northeast of Leoti, Kansas, and Field B is located nearly 17.5 km Northwest of Garden City, Kansas. The East half of the experimental center pivot (Figure 3(c)) is on a quarter section of land that is owned and operated by Kansas State University's Southwest Research and Extension Center (SWREC), located 4.8 km Northeast of Garden City, Kansas. This region is characterized by humid subtropical climate, an average of 35-50 cm annual precipitation, and Richfield series silt-loam soils. During this study, the research plot was primarily used to test different irrigation application technologies, like different nozzle types and application rates. Field A and Field B are characterized by similar soils and climate as those at the SWREC research plot (field (c)). Crop growth stages were monitored during weekly visits to each location.

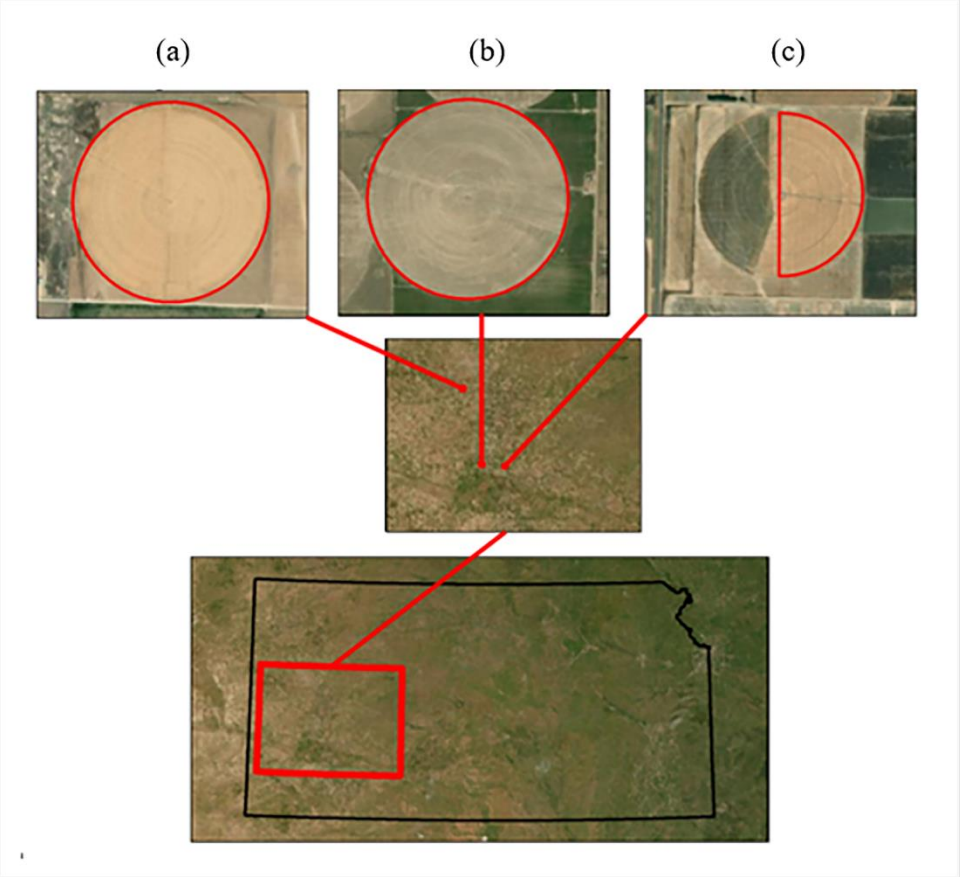

Figure 3. Locations of the center pivots where data was collected (a) Field A (b) Field B and (c) KSU SWREC

3.2 Data Sources and Descriptions

Kansas Mesonet stations located near Field B and the SWREC plot provided daily ET_0 estimates, which were calculated using the ASCE standardized reference evapotranspiration equation (Allen et al., 2005). ET_0 estimates from the Leoti Kansas Mesonet Station located 55 km North of Field A were used in lieu of an on-site mesonet station for Field A. An agricultural technology company provided thermal and multispectral images of each location at a temporal resolution of one week. The spatial resolution of each aerial image varied from 0.8 meter to 1.1 meters by location and collection date based on the elevation of the aircraft-mounted sensors during the data collection flight. Each image was orthorectified and atmospherically corrected by

the agricultural technology company. Each image was reprojected and resampled to the lowest available spatial resolution using tools available in the raster R package (Hijmans, 2020). Reprojecting and resampling these images to the same extent and resolution allows for a pixel-by-pixel comparison of the reflectance values from each measurement date. 30-meter fractional ET images from the Landsat satellite series were downloaded from the EarthExplorer database and are equivalent to crop coefficient maps. This data is provided courtesy of the United States Geological Survey, and was developed by (Senay et al., 2018). The images are available in 298-square-kilometer scenes and can be filtered to only include images with limited cloud coverage. In contrast to the aerial images, which are collected during ideal flight conditions, the Landsat satellites have a fixed return period of about 16 days, meaning images of the fields are not available if the satellite passes over each location on a cloudy day. For this study, the Landsat images were filtered to only include those with 10 % cloud coverage or less. Finally, the spectral resolutions of the aerial imaging platform and Landsat platform vary slightly, but they both measure wavelengths in the near infrared (NIR) and visible red regions of the electromagnetic spectrum.

3.3 Conversion of Vegetation Indices to Crop Coefficients

Pôças et al. (2020) provides a review of techniques and best practices for converting multispectral imagery to single and basal crop coefficients. Their review includes regression equations from existing literature that estimate crop coefficients from NDVI and SAVI. Six of these equations are used to calculate irrigated maize crop coefficients from the aerial and Landsat images described above. Table 1 presents these equations, along with information regarding their development.

Table 1. Linear models correlating corn evapotranspiration coefficients to vegetation indices derived from multispectral reflectance. Adapted from Pôças (2020) to show only equations that apply to irrigated corn.

Reference	Equation*	Remote Sensing Platform	Location	Crop
(Bausch and Neale, 1987)	Kcb = 1.36*NDVI - 0.06	Stationary Radiometer	North Central Colorado	Corn
(Neale et al., 1989)	Kcb = 1.092*NDVI-0.053	Stationary Radiometer	North Central Colorado	Corn
(Neale et al., 1989)	Kcb = 1.181*NDVI-0.026	Stationary Radiometer	Western Colorado	Corn
(Bausch, 1993)	Kcb = 1.416*SAVI+0.017	Stationary Radiometer	North Central Colorado	Corn
(Campos et al., 2017)	Kcb = 1.414*SAVI-0.02	Landsat 5 & 7	Eastern Nebraska	Corn
(Kamble et al., 2013)	Kc = 1.4571*NDVI-0.1725	MODIS	South-Central Nebraska, South Dakota	Rainfed and irrigated agriculture

*Note: Kcb corresponds to the basal crop coefficient, and Kc corresponds to the combined crop coefficient

3.4 Comparison of Aerial and Landsat Data

The aerial multispectral images were converted to NDVI and SAVI using Equations 1 and 2 below, which were originally developed by Rouse et al. (1974) and Huete (1988), respectively. After calculating the NDVI and SAVI values for every pixel in the aerial dataset using Equations 1 and 2 below, the linear equations from Table 1 were used to create maps of crop coefficients. These crop coefficient maps were multiplied by the daily Kansas Mesonet ET_0 to get maps of actual crop ET for each data collection date. Given the differences in spatial and temporal resolutions between these datasets, additional processing was completed to compare the ET maps. To directly compare the aerial and Landsat ET estimates, ET maps from both sources were reprojected to WGS 84 UTM Zone 14N using ArcGIS 10.4.1 (ESRI, 2011) to minimize distortion and clipped to the extent of the irrigated area at each site. The aerial imaging crop coefficient maps were linearly interpolated to a daily time step and multiplied by daily ET_0 values. Interpolation provides a basis for same-day comparisons between the Landsat and aerial ET estimates. Additionally, the aerial maps were chosen over the Landsat maps for interpolation because of their

finer temporal resolution. Interpolating these values between more dates reduces error in the between-flight predictions. Finally, the aerial images were aggregated to a 30-meter resolution by taking the mean crop coefficients from all 0.8-meter pixels that overlapped a given Landsat pixel.

$$NDVI = \frac{NIR-R}{NIR+R} \quad \text{Equation 1}$$

Where:

NDVI = Normalized Difference Vegetation Index

NIR = Percent reflectance of light in the near-infrared region of the electromagnetic spectrum

R = Percent reflectance of light in the red region of the electromagnetic spectrum

$$SAVI = \frac{NIR-R}{NIR+R+L} * (1 + L) \quad \text{Equation 2}$$

Where:

SAVI = Soil Adjusted Vegetation Index

NIR = Percent reflectance of light in the near-infrared region of the electromagnetic spectrum

L = Soil brightness correction factor, assumed to be 0.5 based on

3.5 Delineation of ET Zones

In addition to accurately predicting actual ET, remote sensing platforms must demonstrate sufficient variation in subfield level ET to be useful for VRI scheduling. However, what justifies "sufficient" variation between management zones is highly dependent on the level of control an irrigator has over their pivot system. Two types of control are most common: center pivot speed

control, that creates pie slice shaped VRI zones, and span control that creates concentric gridded VRI zones (Kranz et al., 2012). To mimic VRI schedules for both control techniques, the aerial ET maps were spatially aggregated into VRI zones using two different techniques. Mock pivot speed control zones were created by dividing the center pivots into 2-degree-wide slices, resulting in 90 different VRI zones for the experimental half pivot, and 180 VRI zones for Fields A and B.

K-means clustering was used to build maps of crop water demands useful for systems with zone control, where irrigators can change flow rates to individual spans, or clusters of a few nozzles. The ideal number of clusters for K-means clustering is commonly calculated using the elbow method, which graphs the within-cluster sum of squares for k number of clusters, where k ranges from 1 to some large number, and identifies the point where additional clusters produce minimal reductions in the WSS. K-means clustering, though not a perfect representation of flow control zones given that classifications from high resolution data can produce abnormal shapes, was chosen to maximize the difference in irrigation depths between each zone and mimic the type of zones that would be created from a variable flow control system. K-means clustering is an unsupervised classification technique that assigns each image pixel individually to one of k groups. This is done in iterations, and attempts to minimize within cluster variance, calculated as the within sum of squares (WSS):

$$WSS = \sum_{j=1}^{k} \sum_{i=1}^{n} d(x_i^{(j)}, c_j)^2 \qquad \text{Equation (1)}$$

Where:

WSS = within cluster (or zone) sum of squares

k = number of clusters

n = number of observations in the j^{th} cluster

$x_i^{(j)}$ = i^{th} observation in the j^{th} cluster

c_j = j^{th} cluster centroid

Lastly, the elbow method was used to determine the appropriate number of clusters. The elbow method plots the total WSS for 1 to k clusters. The "elbow" in this line plot corresponds to the location where diminishing reductions in the total WSS occur with increasing k.

Crop coefficient maps using the linear regression equation from Kamble et al. (2013) were used for zone creation since this equation represents a combined soil and crop evapotranspiration coefficient, rather than just a basal crop coefficient. Each zone's irrigation depth was calculated by summing the daily ET maps at the end of every 7-day period after the crop emergence date. The pie zones were aggregated using the mean of all cells in each zone.

3.6 Evaluation of Zone Aggregation Methods

While VRI using these crop coefficients maps does not change the total volume of water used, they could improve how water is allocated within a field if zones are properly delineated. Ideally, these maps would improve water use efficiency, which is defined as the amount of biomass production per unit of water (Briggs & Shantz, 1913). Here, two types of variable rate zone delineations are evaluated based on their ability to account for spatial variability in crop water demands, which is quantified using the mean distance from the centroid. Ideally, variability within each zone (meaning the mean distance from the centroid) will be minimized, and the variability between zones will be maximized. This indicates that the aggregated ET values are an accurate representation of the crop water demands within each zone, and irrigation is properly distributed across the entire field. The mean distance from the centroid is calculated as:

$$J = \frac{1}{k} \sum_{j=1}^{k} \sum_{i=1}^{n} \left| x_i^{(j)} - c_j \right| \qquad \text{Equation (2)}$$

Where:

J = mean distance from the centroid

k = number of clusters (or zones)

n = number of observations in the j^{th} cluster

$x_i^{(j)}$ = i^{th} observation in the j^{th} cluster

c_j = j^{th} cluster centroid

Chapter 5 - Results

4.1 Comparison of Landsat and Aerial Imagery Datasets

Boxplots of mapped crop coefficients for Fields A and B are shown by collection date in Figures 4 and 5. The median crop coefficients from both datasets follow a seasonal pattern similar to traditional crop coefficient curves, with the exception of the July 6th Landsat estimates. These boxplots capture both the spatial and temporal variability in the crop coefficient estimates throughout the growing season. Generally, the interquartile range from the aerial imagery-based estimates appears to decrease for both locations as the season progressed. In comparison, the Landsat-based crop coefficient estimates show consistently wider interquartile ranges throughout the entire growing season. Additionally, the SAVI-based crop coefficients appear to show greater subfield variability later in the season, once the crop canopy is heavily developed.

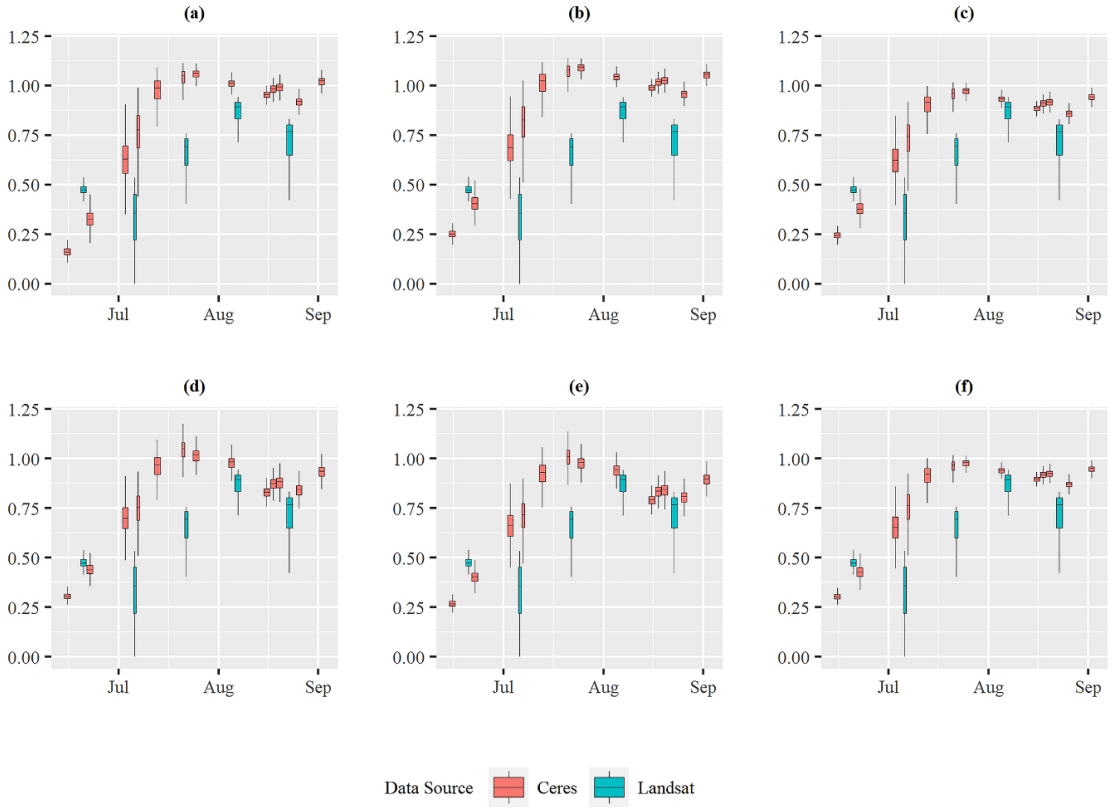

Figure 4. Boxplots of crop coefficients at Field A from Landsat and Aerial imagery. Aerial imaging crop coefficients were calculated from equations developed by (a) Kamble et al. (2013), (b) Bausch (1987), (c) Bausch and Neale (1987) Greeley, CO, (d) Bausch (1993), (e) Campos et al. (2017), and (f) Neale et al. (1989) Fruita, CO

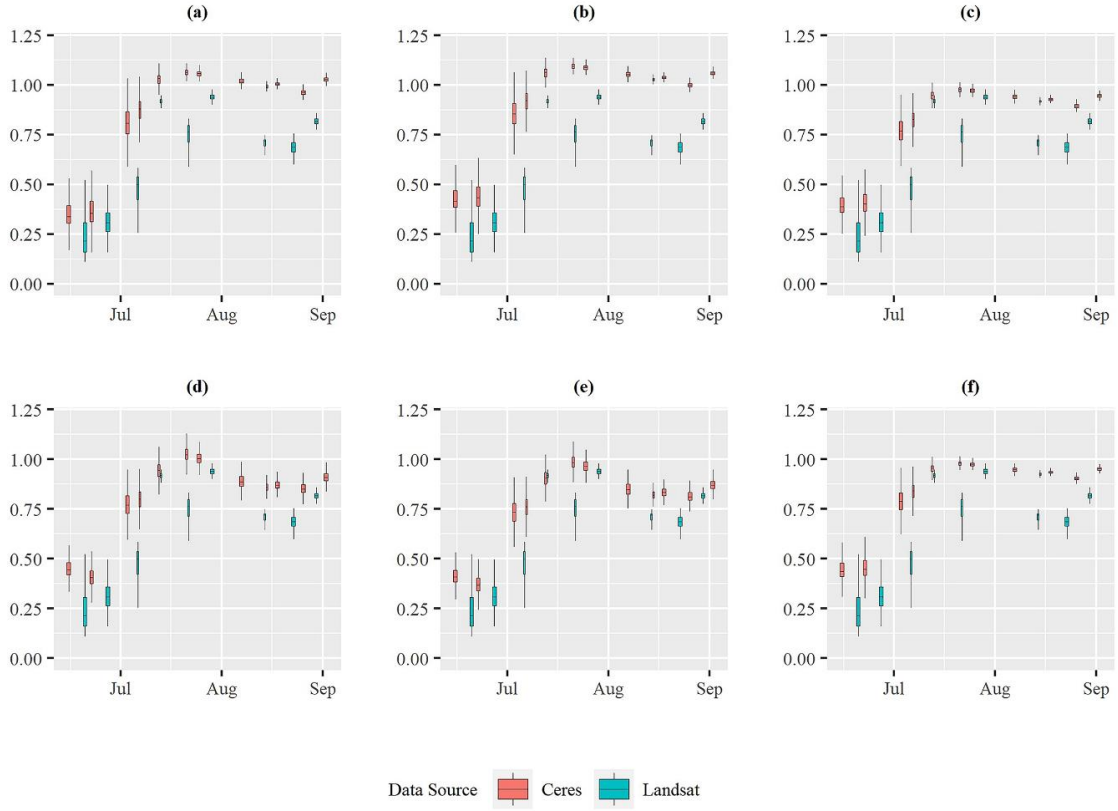

Figure 5. Boxplots of crop coefficients at Field B from Landsat and Aerial Imaging. Aerial imaging crop coefficients were calculated from equations developed by (a) Kamble et al. (2013), (b) Bausch (1987), (c) Bausch and Neale (1987) Greeley, CO, (d) Bausch (1993), (e) Campos et al. (2017), and (f) Neale et al. (1989) Fruita, CO

To better understand what causes these differences, the sum of the differences between all Landsat collection dates were mapped (Figures 6 through 8). The sum of differences was preferred over the sum of squares of the differences to identify parts of each field that were over or underestimated. It was found that differences between the two data sources were consistently greater around field boundaries. Additionally, the Landsat fractional ET estimates most closely approximate the aerial crop coefficients calculated using the regression equation from Kamble et al. (2013).

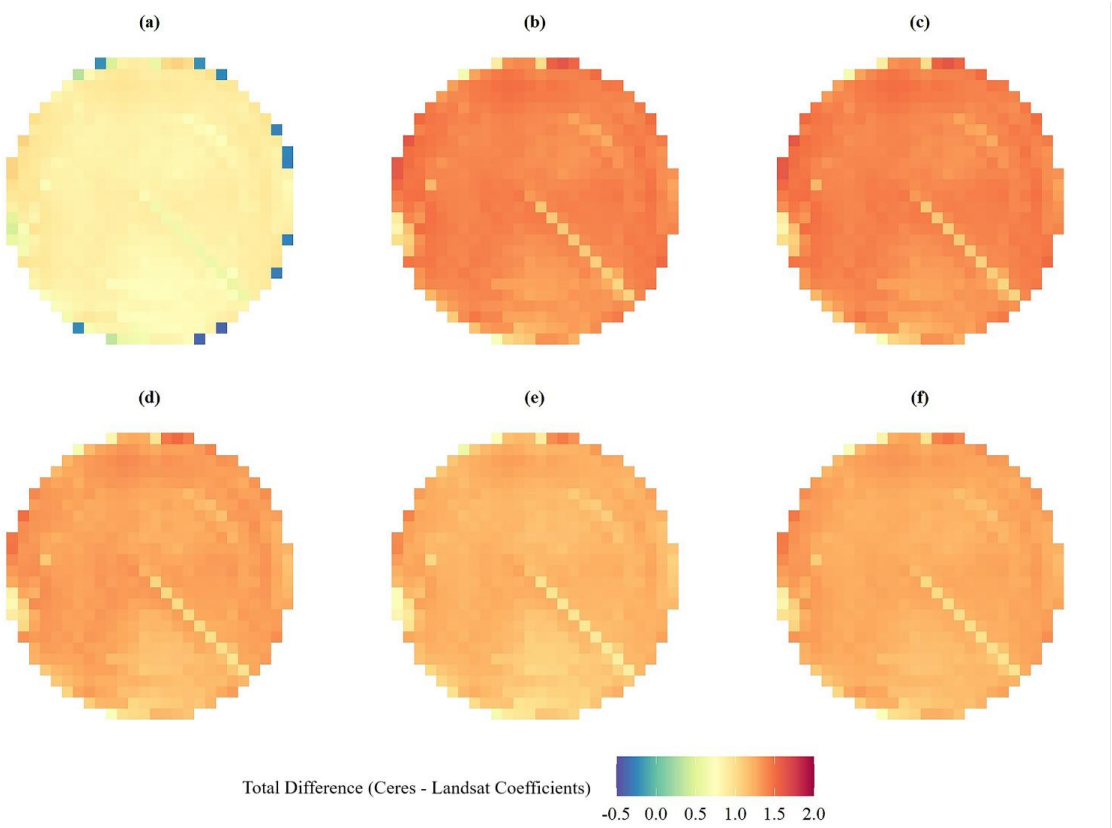

Figure 6. Total seasonal differences between the aerial imaging crop coefficients and the Landsat Fractional ET Data at Field A. Aerial imaging crop coefficients were calculated from equations developed by (a) Kamble et al. (2013), (b) Bausch (1987), (c) Bausch and Neale (1987) Greeley, CO, (d) Bausch (1993), (e) Campos et al. (2017), and (f) Neale et al. (1989) Fruita, CO.

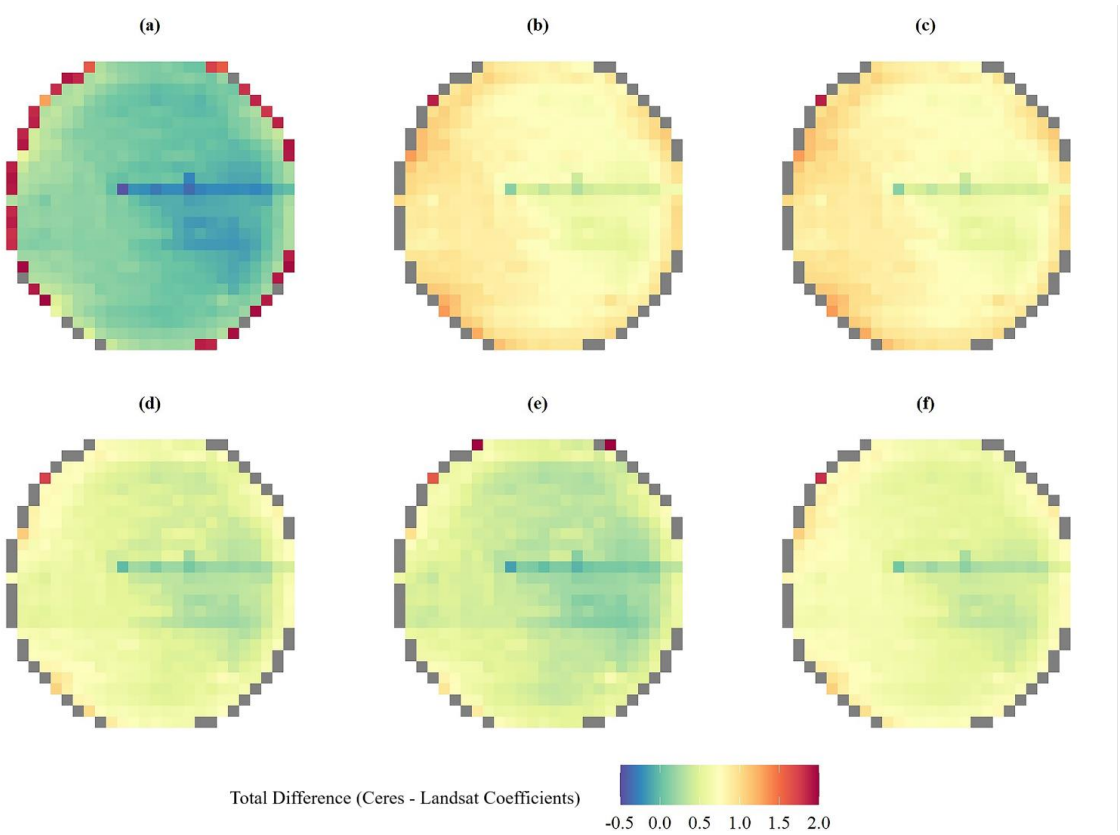

Figure 7. Total seasonal differences between the aerial imaging crop coefficients and the Landsat Fractional ET Data at Field B. Aerial imaging crop coefficients were calculated from equations developed by (a) Kamble et al. (2013), (b) Bausch (1987), (c) Bausch and Neale (1987) Greeley, CO, (d) Bausch (1993), (e) Campos et al. (2017), and (f) Neale et al. (1989) Fruita, CO.

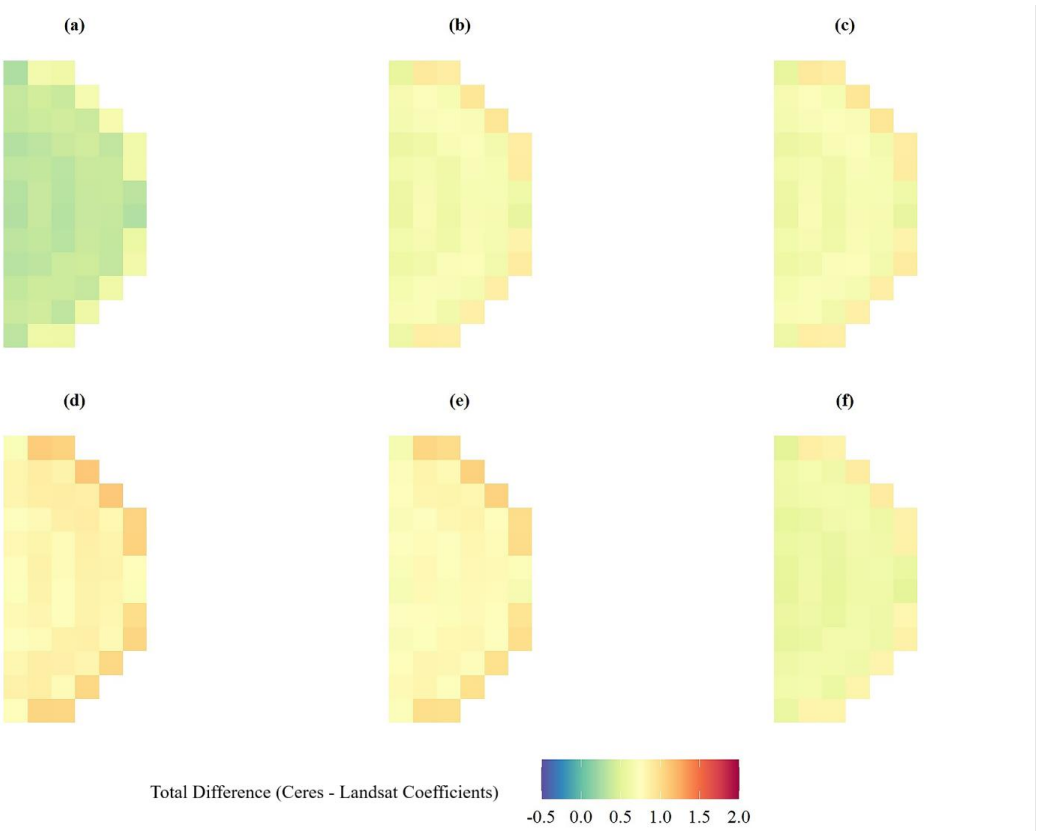

Figure 8. Total seasonal differences between the aerial imaging crop coefficients and the Landsat Fractional ET Data at the SWREC Pivot. Aerial imaging crop coefficients estimates were calculated from equations developed by (a) Kamble et al. (2013), (b) Bausch (1987), (c) Bausch and Neale (1987) Greeley, CO, (d) Bausch (1993), (e) Campos et al. (2017), and (f) Neale et al. (1989) Fruita, CO.

While the maps above identify spatial differences between the Landsat and aerial imaging crop coefficients, they do not demonstrate the impact of differences in crop coefficients on the whole field's evapotranspiration. To better understand the impact of these differences in crop coefficients on the total ET volume, the original 0.8-meter resolution crop coefficient maps were multiplied by the daily ET_0 and raster cell area, then summed. The same process was repeated for the 30-meter crop coefficient maps from the Landsat images to produce a whole-field ET estimate. These whole-field ET estimates are shown in Table 2. It is worth noting that the total ET volume

estimates from the linear models do not appear to be significantly different, indicating that each of the linear models produces relatively similar actual ET estimates.

Table 2. Whole field actual evapotranspiration estimates calculated based on seven different crop coefficient maps. Evapotranspiration depths are in centimeters.

Date	Landsat Fractional ET	Bausch and Neale 1987	Neale et al. 1989 - Greeley	Bausch 1993	Neale et al. 1989 - Fruita	Campos et al. 2017	Kamble et al. 2013
Field B							
06/20/2020	2.604	0.236	0.236	0.274	0.267	0.244	0.170
06/27/2020	3.797	0.432	0.432	0.460	0.452	0.422	0.351
07/06/2020	3.762	0.490	0.490	0.475	0.480	0.442	0.434
07/13/2020	8.275	0.495	0.495	0.472	0.452	0.450	0.470
07/22/2020	7.336	0.688	0.688	0.648	0.622	0.622	0.660
07/29/2020	5.845	0.757	0.757	0.879	0.683	0.848	0.732
08/14/2020	4.036	0.711	0.711	0.663	0.643	0.635	0.683
08/23/2020	5.588	0.569	0.569	0.495	0.521	0.472	0.544
08/30/2020	4.902	0.772	0.772	0.719	0.706	0.686	0.734
Field A							
06/20/2020	3.216	3.416	3.416	3.772	1.948	1.806	1.397
07/06/2020	2.151	6.850	6.850	6.452	3.574	3.419	3.566
07/22/2020	4.402	18.227	18.227	17.582	4.714	4.872	5.088
08/07/2020	5.824	9.032	9.032	8.329	4.554	4.465	4.874
08/23/2020	4.796	10.439	10.439	9.075	4.384	4.016	4.648
SWREC East Pivot							
06/20/2020	0.079	0.088	0.088	0.086	0.103	0.074	0.06
07/06/2020	0.001	0.096	0.096	0.113	0.106	0.103	0.072
07/22/2020	0.053	0.205	0.232	0.208	0.202	0.194	0.18
08/23/2020	0.078	0.372	0.372	0.542	0.335	0.527	0.359

Lastly, the correlation between the aggregated aerial imaging and Landsat crop coefficients estimates was assessed using Pearson's product-moment correlation. Arguably, an equivalence test would be preferred to a correlation test, given the data sources are attempting to measure the same parameter. However, the Landsat and aerial imaging crop coefficients estimates are

calculated using very different methods, and the boxplots (Figures 4 and 5) show little direct equivalence between the data sources. Additionally, a two one-sided equivalence test (TOST) was nonsignificant at an alpha of 0.05, indicating that the two data sources are statistically different. Instead, Pearson's product-moment correlation is calculated to determine if there is a correlation between the crop coefficients from each source. Pearson's coefficient has been commonly used to compare remote sensing data with *in situ* and environmental variables such as evapotranspiration (Szewczak et al., 2020), above ground biomass and canopy height (Li et al., 2016), and land surface temperatures (Mudede et al., 2020). A positive Pearson coefficient close to one indicates a strong, positive correlation between variables, and values near zero indicate there is no correlation between variables. Results from this test showed that the Landsat and aerial imagery-based maps of the crop coefficients were positively correlated at the two producer fields (rho = 0.86 at Field B, 0.63 at Field A) and negatively correlated at the East half SWREC center pivot (rho = -0.95).

4.2 VRI Zone Aggregation Techniques

The variable speed control zone delineation resulted in 180 individual management zones at the producer-owned fields, and 90 management zones at the SWREC half-pivot. An example of these zones is shown in Figure 9. The mean, middle 90%, and total range of weekly ET of these zones is shown for each location in Figures 10-12. At Field A, the mean zone ET ranged from 0.790 cm to 3.17 cm, the middle 90% ranged from 0.725 cm - 0.853 cm to 3.089 cm - 3.214 cm, and the range varied from 0.682 cm - 0.971 cm to 1.992 cm – 3.230 cm between the first and last weeks of the study, respectively. At Field B, the mean zone ET ranged from 1.412 cm to 4.328 cm, the middle 90% ranged from 1.412 cm – 1.896 cm to 4.286 cm – 4.370 cm, and the total range varied from 1.261 cm – 1.896 cm to 4.006 cm – 4.398 cm between the first and last weeks of the studies, respectively. Finally, at the SWREC half-pivot, the mean ET values ranged from 2.084

cm to 6.594 cm, the middle 90% ranged from 2.051 cm – 2.144 cm to 6.409 cm – 6.768 cm, and the total range varied from 2.039 cm – 2.598 cm to 6.268 cm – 6.788 cm between the first and last weeks of the studies, respectively.

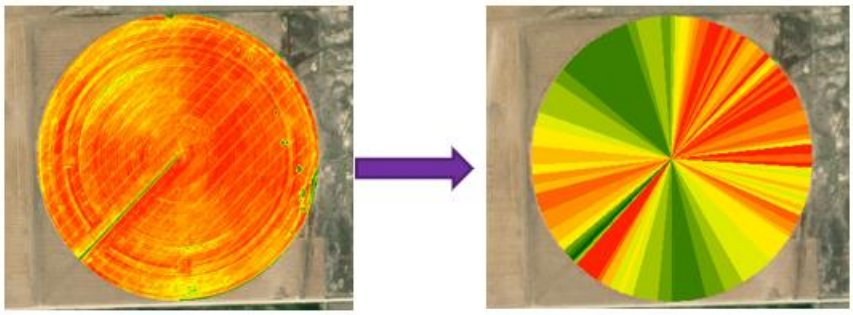

Figure 9. Weekly ET maps (left) are aggregated into variable speed control zones (right) using the mean of all pixels within each zone.

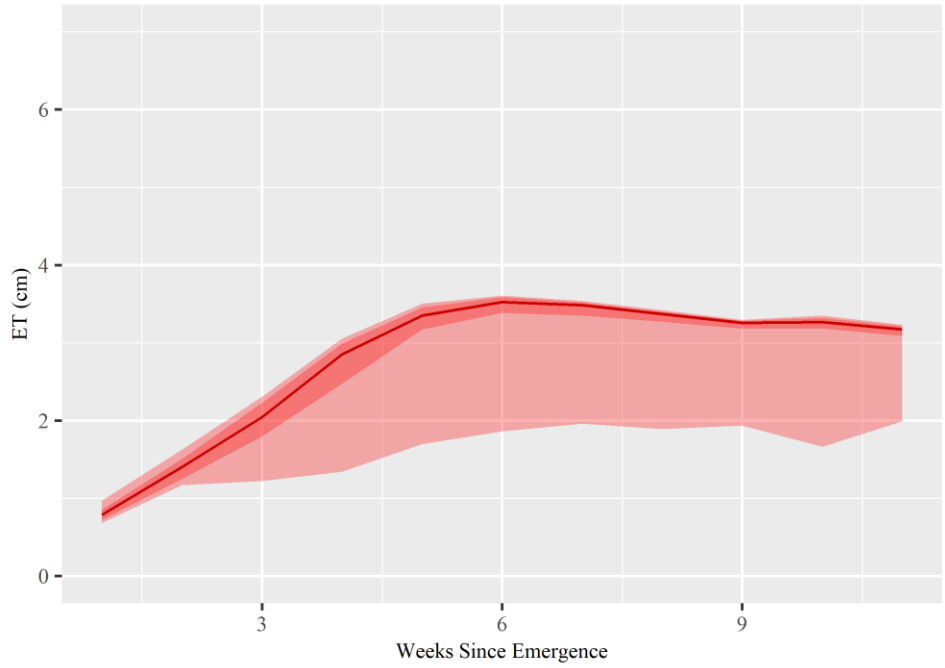

Figure 10. Mean (solid line), middle 90th percentile (dark red zone), and range (light red zone) of weekly evapotranspiration for all variable speed zones in Field A.

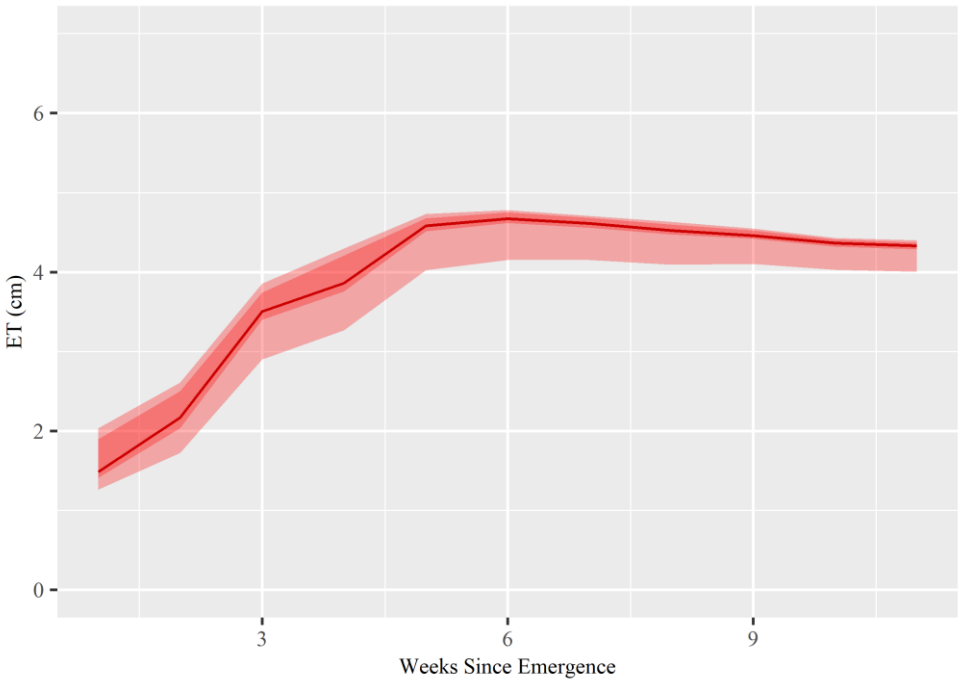

Figure 11. Mean, middle 90th percentile (dark red), and range (light red) of weekly evapotranspiration for all variable speed zones in Field B.

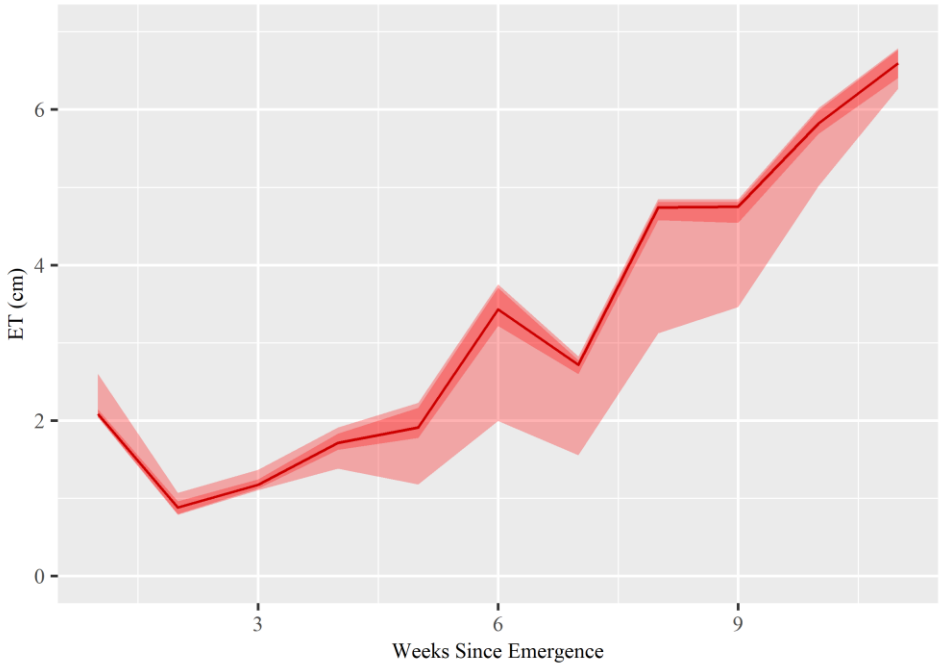

Figure 12. Mean, middle 90th percentile (dark red), and range (light red) of weekly evapotranspiration for all variable speed zones in the SWREC Pivot.

The elbow method described in section was used to determine the appropriate number of K-means clusters for each location and each week. The results for Field B are shown in Figure 13 below. This graph shows that four clusters are sufficient for every week during the data collection period at Field B, given that any additional clusters produce a minimal reduction in WSS. The same graphs for the other two locations yielded similar results, with four clusters being sufficient for K-means clustering every week. The largest WSS occurred between two and four weeks after emergence for both Field A and Field B. In contrast, the largest WSS at the SWREC field occurred between seven and nine weeks after emergence. The WSS at the SWREC likely peaked later in the season due to a malfunctioning section of nozzles on the center pivot, which stunted the growth of a large section of plants in the middle of the pivot and increased the subfield crop coefficients variability.

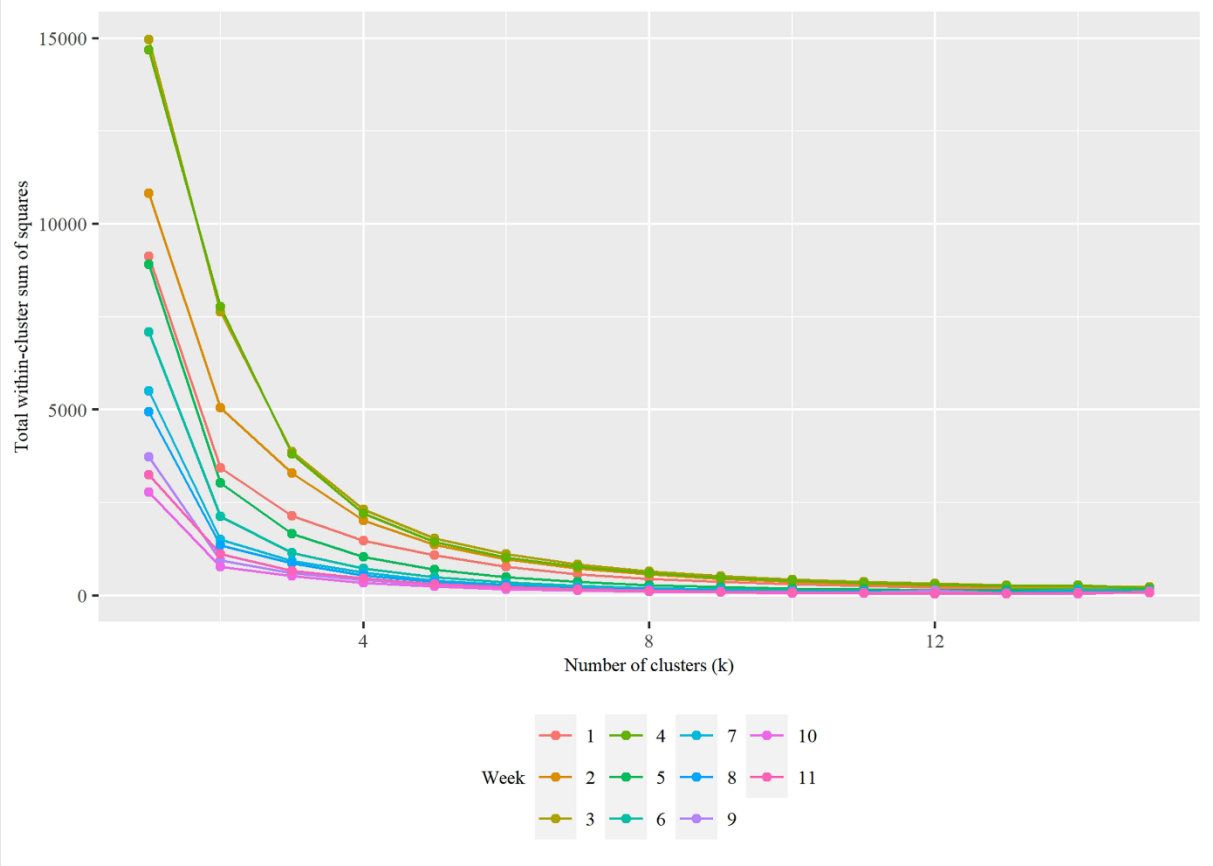

Figure 13. Elbow test results for Field B by week

The centroid, or mean, value of all weekly ET pixels in each cluster was used to determine the weekly crop water demand in each zone. The weekly crop demand for each zone is shown in

Figure 14. Weekly ET maps (left) are aggregated using K-means clustering to mimic variable flow control zones (right).

Table 3, and an example of a K-means clustering map is shown in Figure 14. Note that unlike the pivot speed control zones, the size and shape of each K-means cluster changes every week because the ET maps themselves are used for the VRI zone delineation. As expected, the area with the largest weekly ET tended to grow as the season progressed, which corresponds to

increased crop water demands with crop maturity. By six weeks after emergence at both the Water Tech Farms, the K-means zone with the highest weekly ET covered about 70% of the entire field. Lastly, the average mean distance from the centroid for each aggregation method at each location is shown in Figures 15-17 for comparison.

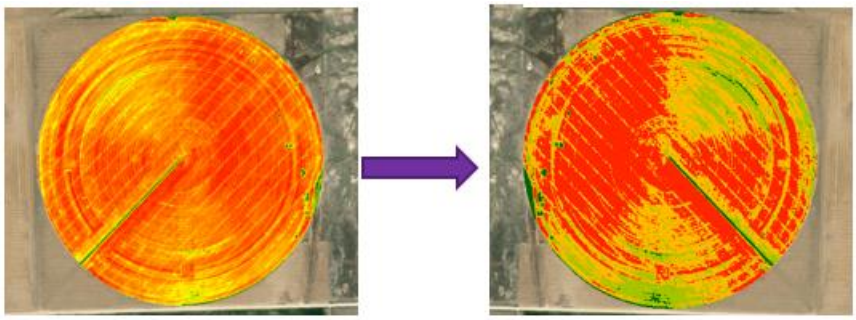

Figure 14. Weekly ET maps (left) are aggregated using K-means clustering to mimic variable flow control zones (right).

Table 3. Evapotranspiration depth (centimeters) for every K-means clustering zone, sorted by minimum depth to maximum depth

Field B

Weeks Since Emergence	Minimum	→		Maximum
1	1.295	1.556	1.884	2.337
2	0.986	1.966	2.293	2.683
3	1.510	3.006	3.483	3.825
4	1.832	3.417	3.881	4.238
5	2.030	3.717	4.455	4.680
6	1.800	3.673	4.526	4.730
7	1.873	3.715	4.550	4.674
8	1.741	3.647	4.482	4.599
9	1.812	3.503	4.421	4.514
10	2.173	3.545	4.307	4.404
11	2.194	3.938	4.288	4.391

Field A

1	0.683	0.806	0.952	1.943
2	1.107	1.304	1.472	1.673
3	1.400	1.803	2.096	2.391
4	1.114	2.264	2.721	3.077
5	1.253	2.763	3.229	3.498
6	1.341	2.838	3.382	3.591
7	1.384	2.666	3.329	3.526
8	1.400	2.548	3.217	3.414
9	1.364	2.321	3.122	3.290
10	1.242	2.389	3.124	3.319
11	1.325	2.450	3.034	3.219
SWREC East Pivot				
1	2.032	2.108	2.261	2.616
2	0.762	0.864	0.991	1.143
3	1.067	1.168	1.295	1.549
4	1.473	1.676	1.829	2.057
5	1.372	1.778	2.057	2.388
6	2.286	2.997	3.556	4.064
7	1.651	2.235	2.692	3.023
8	2.769	3.835	4.496	5.055
9	2.642	3.835	4.470	4.928
10	3.505	5.055	5.613	5.994
11	4.343	5.944	6.477	6.756

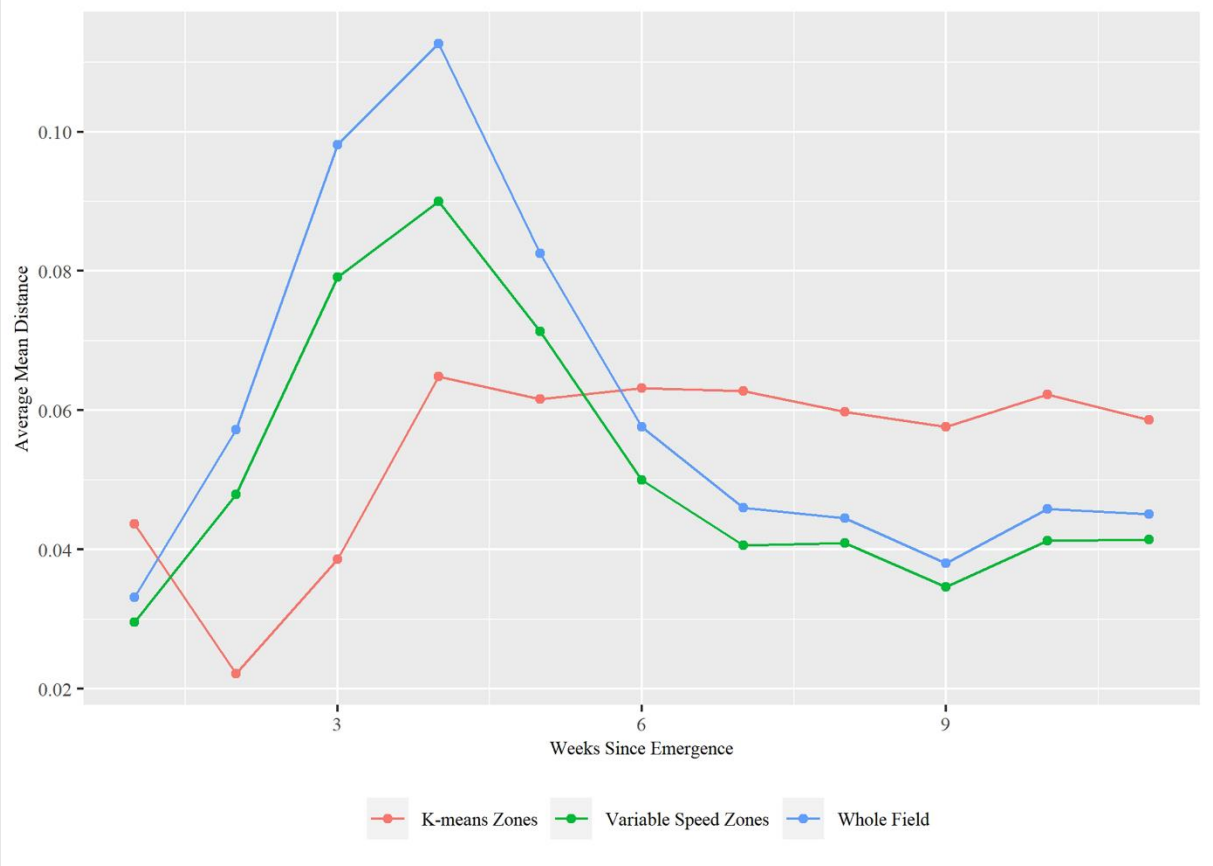

Figure 15. Time series of average mean distance from the zone's aggregated ET value by aggregation method at Field A. The average mean distance from the average whole-field ET is included for reference.

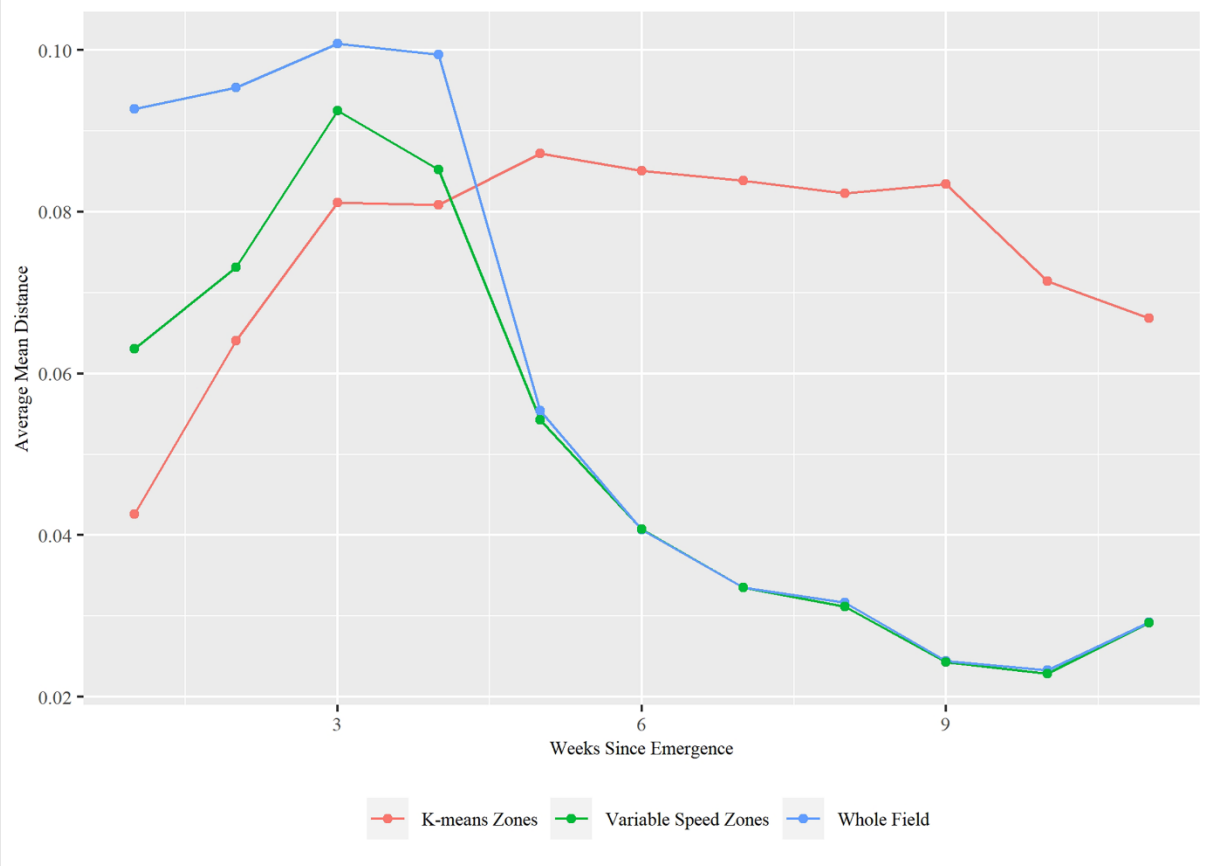

Figure 16. Time series of average mean distance from the zone's aggregated ET value by aggregation method at Field B. The average mean distance from the average whole-field ET is included for reference.

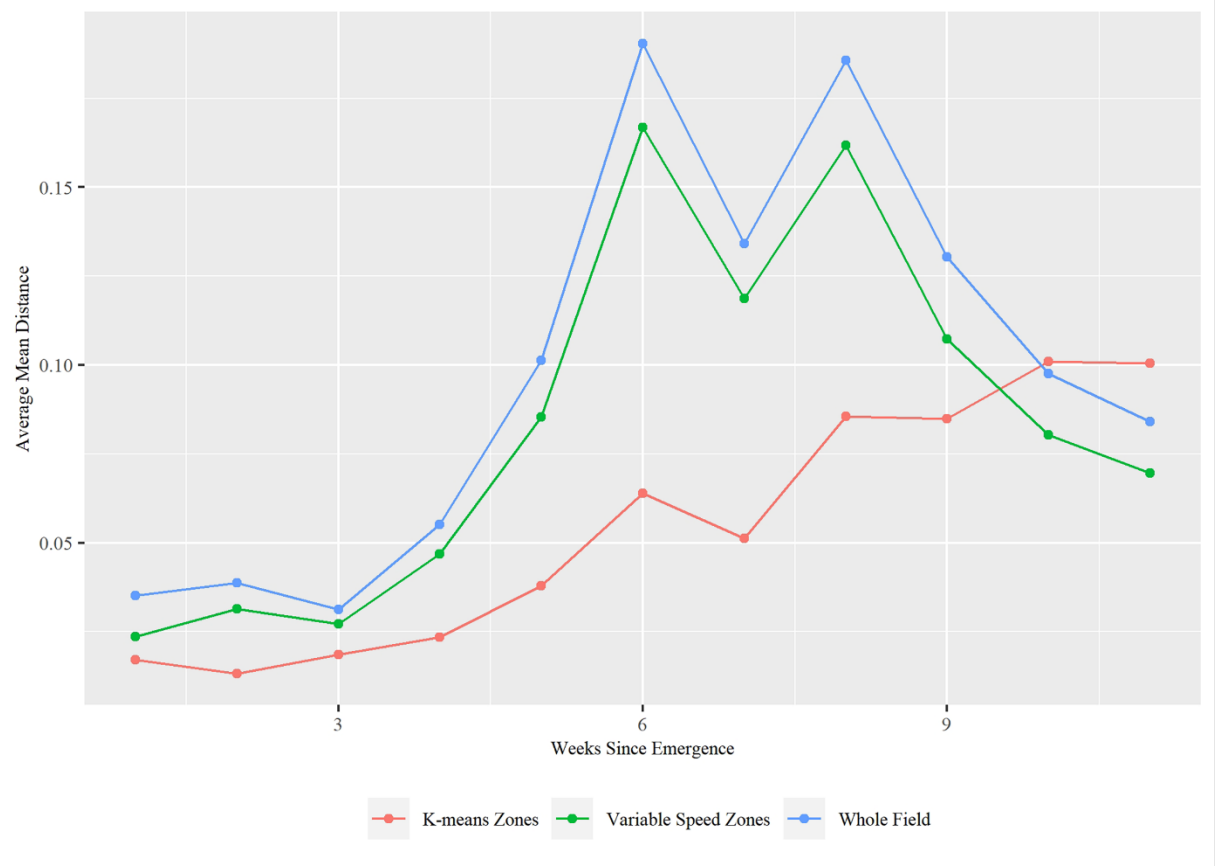

Figure 17. Time series of average mean distance from the zone's aggregated ET value by aggregation method at the SWREC Pivot. The average mean distance from the average whole-field ET is included for reference.

The range of mean distances from the centroid varied by date and aggregation type. The range of mean distances was much greater in the variable speed zones than in the K-means clusters. Even though the average mean distance from the centroid in the K-means clusters was greater than in the variable speed zones, there was higher variability in the mean distances in the variable speed zones. This means K-means clustering produced zones with similar levels of within-zone variability, while the variable speed zones had inconsistent levels of within-zone variability. The causes and implications of this phenomenon are discussed further in the next chapter.

Chapter 6 - Discussion

5.1 Comparison of Landsat and Aerial Imagery Data for ET Estimation

The first goal of this research was to understand differences between sub-field crop coefficient estimates from two remote sensing platforms—the Landsat Satellites and aerial imagery. The first set of crop coefficients estimates were obtained from the Landsat Provisional ET Dataset, which uses the Operational Simplified Surface Energy Balance (SSEBop) (Senay, 2018; Senay et al., 2013) to estimate fractional ET. The second set of crop coefficients estimates was calculated using multispectral imagery from sensors mounted on manned aircraft, and six different linear regression models that calculate basal and combined crop coefficients from multispectral indices. This research was conducted at three irrigated corn fields in Western Kansas. Overall, comparing these two remote sensing data sets proved to be incredibly challenging based on their differences in spatial resolutions and revisit periods. These differences resulted in data from each source being collected on asynchronous days and at different spatial resolutions. Linear interpolation and spatial aggregation techniques were used to create images on the same calendar day and the same spatial resolution, providing a more accurate comparison of the two estimates. A major limitation to this comparison was a lack of same-day data collection between the datasets. To account for this, the aerial images were linearly interpolated between collection dates and aggregated to a 30-meter resolution to match the Landsat data. It is also worth noting that the SSEBop model used to create the Landsat Provisional ET Dataset was developed across the contiguous United States, and is commonly used for regional studies, but has not been evaluated at the sub-field level.

All the linear regression equations and data combinations produced higher ET estimates than the Landsat data. Of these combinations, the regression equation from Kamble et al. (2013)

provided the closest estimates to the Landsat data. This is likely because the Kamble et al. equation predicts the combined crop coefficient, which accounts for both soil and plant transpiration, compared to the other equations which only predict the basal crop coefficient. The NDVI-based linear models predicted less variability in crop coefficients than the SAVI-based linear models and satellite-based crop coefficients. This is a phenomenon noted by Neale et al. (1989), who found that NDVI-crop coefficient relationships are not accurate past effective cover development. This is likely because NDVI becomes insensitive to differences in canopy coverage past a leaf area index of 2-3 (Myneni et al., 1997).

Spatially, the greatest differences between these two data sets occurred around the field boundaries. This is likely due to the difference in spatial resolutions of the datasets. The higher resolution aerial images provide a more accurate delineation of the boundary between crops and the surrounding unplanted area. This concept of "mixed pixels" is common to studies using remote sensing data and is further discussed in relation to agricultural management practices by (Ines & Honda, 2005). The unplanted areas around the center pivot boundaries have lower crop coefficients since they are not heavily vegetated. Therefore, the lower resolution Landsat images may be under-predicting the crop coefficients at the field boundaries, given that a single Landsat pixel includes both planted and unplanted land.

Comparing the two datasets on a paired pixel-by-pixel basis demonstrated poor agreement between the Landsat and crop coefficients estimates, with a two one-sided equivalence test concluding that the datasets are statistically different at an alpha of 0.05. However, a correlation test using Pearson's rho demonstrated that the interpolated and aggregated crop coefficients estimates from the aerial images were moderately, and positively correlated to the Landsat Fractional ET estimates at the two producer fields (rho = 0.86 at Field B, 0.63 at Field A) and

negatively correlated at the SWREC center pivot (rho = -0.95). The positive rho values close to 1 from Fields A and B indicate that the crop coefficients estimates from the two data sources were positively linearly correlated, meaning as the estimated crop coefficients from one data source increases, so does the estimated crop coefficients from the other. The strong negative rho value at the SWREC indicates that the crop coefficients from the two data sources were negatively linearly correlated. However, the SWREC field was much smaller, meaning there were fewer data points for a pixel-by-pixel comparison. This means that the confidence intervals of the rho estimate at the SWREC plot had a wider confidence interval. Additionally, the SWREC center pivot uses dragon lines, which drastically decreases evaporation rates from soil and crop canopies. This may have led to largely inaccurate crop coefficients from one or both data sources, and the results from the SWREC plot should be interpreted with this difference in management practices in mind.

While both data sources demonstrated variability in ET at the subfield level, there are some practical limitations to using either dataset for variable rate irrigation scheduling. The most significant limitation for both datasets is a lack of validation from *in situ* measurements. While this is an important step for utilization in VRI scheduling, this study aimed only to assess the differences between, and spatial variability of, the two data sets. While other researchers have used aerial imagery data to help monitor water stress in almond and pistachio orchards (Bellvert et al., 2018), it has not been validated for corn with the methods described above.

Likewise, the Landsat images have been validated using data at regional scales, but they have not been used for sub-field level management decisions (Senay et al., 2016, 2017; Singh et al., 2014). The second major limitation is the image processing time, which ranges from about 1-2 days for the aerial images, to about a week for the Landsat images. It is imperative for irrigators to make decisions at the right time to avoid crop stress that could negatively impact yields,

especially during the reproductive growth stages. Third, aerial imaging provides a wide variety of products for both water and nutrient stress monitoring, as well as customized insight into their data. However, for some, these services may not be cost effective at the frequency needed for irrigation scheduling. In contrast, the Landsat Provisional ET Dataset is available for free, but the raw data does not have the same level of support or insight that aerial imagery provides. Additionally, the Landsat satellites have a fixed revisit period, meaning they may not always collect data under ideal environmental conditions (i.e. rainy or cloudy days).

5.2 VRI Zone Aggregation Techniques

Aggregating crop coefficients maps using the methods presented here allows irrigators to turn remotely sensed data into clear, actionable management decisions. However, the size and shape of VRI zones is dependent on an irrigator's level of control over their center pivot. For an aggregation technique to be effective, the variation between zones must be greater than any natural fluctuations in the center pivot's flow rate under uniform application irrigation. Additionally, the prescribed irrigation depth must be representative of each zone, meaning the variability within each zone should be minimized. This allows irrigators to properly distribute water across their field and maintain high yields under water-limited conditions. Two different aggregation techniques: 2-degree-wide pivot speed control zones, and K-means clustering were tested in this study. Irrigation depths for each zone were calculated and within-zone variability was assessed using the mean distance from the centroid.

It was found that, at both the water technology farms, peak weekly ET volume was reached at around six weeks after emergence. In contrast, the SWREC East Pivot ET continued to increase throughout the data collection period due to the malfunctioning nozzles, which stunted a portion of the field's growth until late in the season. The weekly ET between the middle 90th percentile

of the variable speed zones (or the middle 162 zones), differed by 0.254-0.508 cm. for the first five weeks after emergence, then decreased to less than 0.254 cm. for the remainder of the data collection at all locations. However, the total range of all zones' ET values ranged from about 1.27 cm at Field B, to about 1.905 cm at Field A and the SWREC East Pivot. These differences correspond to 10-20% difference in irrigation depth for the middle 90th percentile of all zones during the first five weeks after emergence, and a 30-50% difference in irrigation depth between the minimum and maximum ET zones for most of the data collection period. Overall, this demonstrates that there is a clear difference in the sub-field zone ET depths. However, sub-field ET tends to become more uniform in irrigated agriculture as the season progresses. These early season ET maps may help irrigators allocate resources under water-limited conditions to relieve prolonged early-season water stress, which negatively impacts final yields (Çakir, 2004; NeSmith & Ritchie, 1992).

The K-means clustering produced the lowest average mean distance from the centroid--but only for the first few weeks after emergence. After the fifth week post-emergence, the variable speed control zones produced the lowest average mean distance from the centroid, which was close to the whole-field average mean distance from the centroid. Analyzing the mean distance from the centroids revealed that the K-means cluster that corresponded to the lowest irrigation depth consistently had the greatest mean distance from the centroid. This cluster represented the most barren parts of the fields, including the center pivot access roads and highly damaged planted areas within the pivot circle. Weeks one to four had the greatest average mean distance from the centroid for the whole field, and the variable speed control zones. This indicates that the spatial variability within the field is typically the highest within the first month after emergence.

Analysis of the average mean distance from the centroid also revealed that the within-zone variability was more consistent in the K-means zones than in the variable speed zones. This means that even though the variable speed zones had a lower average mean distance from the centroid during the second half of the data collection period, the range of mean distances was much wider. This indicates that the mean ET in at least a few of the variable speed zones did not accurately represent the water demand in those zones. This is likely due to the static nature of the variable speed zones. Some of the variable seed zones contain both healthy and unhealthy or unplanted areas. Evapotranspiration increases in healthy planted areas as the season progresses, while the evapotranspiration in unplanted or damaged areas remains low. This means that the variability within variable speed zones that cover both healthy and unhealthy areas will increase. However, the K-means clustering method adjusts to the changing crop growth by changing the zone boundaries. In both aggregation methods at Field A and Field B, the range of mean distances tended to increase for the first three to five weeks after emergence, then remained relatively consistent for the rest of the season.

5.3 Future Work

This work presents several opportunities for future research to improve on the comparison of crop evapotranspiration monitoring using remote sensing platforms. First, the introduction of additional uncertainty could be reduced by carefully planning data collection to occur on the same date, and as close to the same time, for all data sources. This would eliminate the need to perform temporal interpolation between collection dates, which simplifies data processing needs. Second, all imaging platforms useful at the sub-field scale should be able to identify unplanted regions, like pivot access roads. These areas were not filtered out of our data analysis, but they should be when evaluating subfield crop water demands. As demonstrated here, K-means clustering can identify

these regions. Performing K-means clustering once to remove unplanted areas from ET maps would improve management zone delineations. Third, the inclusion of *in situ* measurements would provide a more established baseline for comparing ET estimates from remotely sensed imagery. Two methods could be used for this validation. The first would use a series of eddy covariance towers to measure energy fluxes at multiple locations in the field and directly calculate ET, similar to the methods described in Suyker & Verma (2009). The second would use a combination of soil moisture probes, rain gauges, and crop models to estimate ET from a soil water balance equation. Fourth, research investigating the use of other multispectral vegetation indices might help quantify spatial variability in crop water demands after full canopy development. In this study, the linear models that used NDVI images to predict crop coefficients resulted in little variability during the late season. However, the satellite images captured greater variability in the late season, demonstrating that other reflectance-based relationships to crop coefficients might capture spatial variability in ET more accurately later in the growing season.

The goal of VRI is to properly allocate water within a field to prevent over and under irrigation. This reduces waste while maintaining high yields under water limited conditions. However, this study did not quantify the impacts of scheduling irrigation using these data sources on crop yields or water use efficiency. Therefore, further research is needed to determine if VRI schedules built using these high-resolution ET maps improve water use efficiency. This could be accomplished using field trials and live scheduling using the crop coefficients maps. However, this is relatively resource intensive. Instead, the researchers recommend adapting existing crop models, like DSSAT to include spatially variable crop coefficients. This would serve as an intermediate test before implementing this scheduling method in the physical world. This was briefly attempted by the researchers using the GeoSim extension for DSSAT (Thorp & Bronson, 2013), but these

modifications require special consideration regarding discrepancies between the modeled and measured parameters, such as emergence timelines. This study investigated two types of VRI zone delineation, and future research is required to compare additional zone delineation methods that balance equipment capabilities with spatial variability in crop water demands. Further, a cost analysis of using these remotely sensed images for VRI scheduling is important to encourage the widespread adoption of these remote sensing data sources for VRI scheduling. While this research used images collected by an agricultural technology company on a weekly basis, less frequent data collection might reduce the cost to consumers and still provide insight into crop water demands for irrigation scheduling. This research showed that this may be especially true after five to seven weeks post-emergence, when the spatial variability of ET decreases in well-irrigated fields. However, if irrigators expect some level of stunted growth in certain parts of their field, as is common with hail damage or malfunctioning equipment, then they would likely benefit from regular data collection further into the season.

Chapter 7 - Conclusion

This work investigated sub-field evapotranspiration estimates on three irrigated corn fields in Western Kansas, all of which depend on the High Plains Aquifer for water. This research used data from two remote sensing platforms, and two common aggregation techniques to predict weekly ET, and delineate variable rate irrigation zones. Six linear VI-crop coefficients models paired with aerial imagery estimated higher ET rates than the Landsat Provisional Actual ET dataset. Comparing these two data sources in-depth proved challenging based on their differences in temporal and spatial resolutions. However, Pearson's product-moment correlation tests showed moderate levels of correlation between VI-crop coefficients model outputs and Landsat's fractional ET layer. The two aggregation techniques--variable speed zones and K-means

clustering--both reduced sub-field level ET variability and demonstrated potential for use in VRI scheduling. The variable speed zones require minimal equipment adjustments for use, but do not always accurately represent crop water demands in every zone. In contrast, the K-means clusters require irrigators to have control of flow rates to individual spans, or groups of nozzles. K-means clustering also evenly distributed the within-zone variability between each zone rather than creating a few zones with much higher variability, like in the variable speed zones. More research investigations are needed before these sub-field crop coefficients maps can get integrated into an automated irrigation scheduling tool. However, this study demonstrate variability in subfield-level ET zones that warrants further research into the topic. Critical areas of future research include validating these data sets with *in situ* measurements and quantifying the yield and financial benefits relative to uniform irrigation schedules.

References

Abioye, E. A., Abidin, M. S. Z., Mahmud, M. S. A., Buyamin, S., Ishak, M. H. I., Rahman, M. K. I. A., . . . Ramli, M. S. A. (2020). A review on monitoring and advanced control strategies for precision irrigation. Computers and Electronics in Agriculture, 173, 105441. https://doi.org/10.1016/j.compag.2020.105441https://doi.org/10.1016/bs.agron.2020.03.001

Ajaz, A., Datta, S., & Stoodley, S. (2020). High Plains Aquifer–State of Affairs of Irrigated Agriculture and Role of Irrigation in the Sustainability Paradigm. *Sustainability*, *12*(9), 3714. https://doi.org/10.3390/su12093714

Allen, R. G., Pereira, L. S., Smith, M., Raes, D., & Wright, J. L. (2005). FAO-56 dual crop coefficient method for estimating evaporation from soil and application extensions. *Journal of Irrigation and Drainage Engineering*, 131(1), 2–13. https://doi.org/10.1061/(ASCE)0733-9437(2005)131:1(2)

Andrade, M. A., O'Shaughnessy, S. A., & Evett, S. R. (2020). ARSPIVOT, A sensor-based decision support software for variable-rate irrigation center pivot systems: Part A. Development. *Transactions of the ASABE*, 63(5), 1535–1547.

Baumhardt, R. L. (2003). Dust bowl era. *Encyclopedia of water science*, *491*.

Bausch. (1993). Soil background effects on reflectance-based crop coefficients for corn. *Remote Sensing of Environment*, 46(2), 213–222.

Bausch & Neale. (1987). Crop coefficients derived from reflected canopy radiation: A concept. *Transactions of the ASAE*, 30(3), 0703–0709. https://doi.org/10.13031/2013.30463

Bellvert, J., Adeline, K., Baram, S., Pierce, L., Sanden, B. L., & Smart, D. R. (2018). Monitoring crop evapotranspiration and crop coefficients over an almond and pistachio orchard throughout remote sensing. *Remote Sensing*, 10(12), 2001. https://doi.org/10.3390/rs10122001https://doi.org/10.1016/j.envsoft.2013.09.002

Blatchford, M. L., Mannaerts, C. M., Zeng, Y., Nouri, H., & Karimi, P. (2019). Status of accuracy in remotely sensed and in-situ agricultural water productivity estimates: A review. *Remote Sensing of*

Environment, *234*, 111413. https://doi.org/10.1016/j.rse.2019.111413

Blonquist Jr., J. M., Jones, S. B., & Robinson, D. A. (2005). A time domain transmission sensor with TDR performance characteristics. *Journal of Hydrology*, 314(1), 235–245. https://doi.org/10.1016/j.jhydrol.2005.04.005

Briggs, L. J., & Shantz, H. L. (1913). The water requirement of lants. U.S. Government Printing Office.

Buchanan, R., Buddemeier, R. W., & Wilson, B. B. (2001). *The high plains aquifer*. Kansas Geological Survey Lawrence, KS.

Burke, J. J. (1993). Thermal kinetic windows of plant enzymes. *Biotechnology for arid plants*, 73-82.

Çakir, R. (2004). Effect of water stress at different development stages on vegetative and reproductive growth of corn. *Field Crops* Research, 89(1), 1–16. https://doi.org/10.1016/j.fcr.2004.01.005

Calera, A., Campos, I., Osann, A., D'Urso, G., & Menenti, M. (2017). Remote Sensing for Crop Water Management: From ET Modelling to Services for the End Users. *Sensors*, *17*(5), 1104. https://doi.org/10.3390/s17051104

Campos, I., Neale, C. M. U., Suyker, A. E., Arkebauer, T. J., & Gonçalves, I. Z. (2017). Reflectance-based crop coefficients REDUX: For operational evapotranspiration estimates in the age of high producing hybrid varieties. *Agricultural Water Management*, 187, 140–153. https://doi.org/10.1016/j.agwat.2017.03.022

Çakir, R. (2004). Effect of water stress at different development stages on vegetative and reproductive growth of corn. *Field Crops* Research, 89(1), 1–16. https://doi.org/10.1016/j.fcr.2004.01.005

Casanova, J. J., Evett, S. R., & Schwartz, R. C. (2012). Design of access-tube TDR Sensor for soil water content: Testing. *IEEE Sensors Journal*, 12(6), 2064–2070. https://doi.org/10.1109/JSEN.2012.2184282

Colaizzi, P.D., C.Y. Choi, P.M. Waller, E.M. Barnes, Clarke, T.R. (2000). Determining irrigation management zones in precision agriculture using the water deficit index at high

spatial resolutions. 2000 ASAE Annual International Meeting. Pp. 1-19.

Cotterman, K. A., Kendall, A. D., Basso, B., & Hyndman, D. W. (2018). Groundwater depletion and climate change: Future prospects of crop production in the Central High Plains Aquifer. *Climatic Change*, *146*(1–2), 187–200. http://dx.doi.org.er.lib.k-state.edu/10.1007/s10584-017-1947-7

Daponte, P., De Vito, L., Glielmo, L., Iannelli, L., Liuzza, D., Picariello, F., & Silano, G. (2019). A review on the use of drones for precision agriculture. *IOP Conference Series: Earth and Environmental Science*, *275*, 012022. https://doi.org/10.1088/1755-1315/275/1/012022

Doorenbos, J., & Pruitt, W. O. (1975). Guidelines for predicting crop water requirements (FAO Irrigation and Drainage Paper 24). *Food and Agriculture*. Organization of the United Nations, Rome, Italy.

ESRI 2011. ArcGIS Desktop: Release 10.4.1 Redlands, CA: Environmental Systems Research Institute.

Evans, R. G., & King, B. A. (2012). Site-Specific sprinkler irrigation in a water-limited future. *Transactions of the ASABE*, 12.

Elliott, J., Deryng, D., Müller, C., Frieler, K., Konzmann, M., Gerten, . . . Wisser, D. (2014). Constraints and potentials of future irrigation water availability on agricultural production under climate change. *Proceedings of the National Academy of Sciences*, *111*(9), 3239–3244. https://doi.org/10.1073/pnas.1222474110

Elshall, A. S., Arik, A. D., El-Kadi, A. I., Pierce, S., Ye, M., Burnett, K. M., . . . Chun, G. (2020). *Groundwater sustainability: A review of the interactions between science and policy*. *15*(9), 093004. https://doi.org/10.1088/1748-9326/ab8e8c

Evans, R. G., & King, B. A. (2012). Site-specific sprinkler irrigation in a water-limited future. *Transactions of the ASABE*, 12.

Evett, S. R., O'Shaughnessy, S. A., & Peters, R. T. (2014). Irrigation scheduling and supervisory control data acquisition system for moving and static irrigation systems. U.S. Patent No. 8,924,031 B1.

Evett, S. R., O'Shaughnessy, S. A., Andrade, M. A., Colaizzi, P. D., Schwartz, R. C., Schomberg, H. S., … Sui, R. (2020). Theory and development of a VRI decision support system: The USDA-ARS ISSCADA

approach. *Transactions of the ASABE*, 63(5), 1507–1519.

Evett, S. R., Schwartz, R. C., Tolk, J. A., & Howell, T. A. (2009). Soil profile water content determination: Spatioteporal variability of electromagnetic and neutron probe sensors in access tubes. *Vadose Zone Journal*, 8(4), 926–941. https://doi.org/10.2136/vzj2008.0146

Glenn, E. P., Neale, C. M. U., Hunsaker, D. J., & Nagler, P. L. (2011). Vegetation index-based crop coefficients to estimate evapotranspiration by remote sensing in agricultural and natural ecosystems. *Hydrological Processes*, *25*(26), 4050–4062. https://doi.org/10.1002/hyp.8392

Godfray, H. C. J., Beddington, J. R., Crute, I. R., Haddad, L., Lawrence, D., Muir, J. F., Pretty, J., Robinson, S., Thomas, S. M., & Toulmin, C. (2010). Food Security: The Challenge of Feeding 9 Billion People. *Science*, *327*(5967), 812–818.

Golden, B. (2016). Monitoring the impacts of Sheridan County 6 local enhanced management area.

Golden, B. B., & Leatherman, J. C. (2019). Impact analysis of the walnut creek intensive groundwater use control area. Journal of Regional Analysis & Policy, 47(2), 176-187.

Griggs, B. (2014). Lessons from Kansas: a more sustainable groundwater management approach. Water in the West.

Gu, Z., Qi, Z., Burghate, R., Yuan, S., Jiao, X., & Xu, J. (2020). Irrigation Scheduling Approaches and Applications: A Review. *Journal of Irrigation and Drainage Engineering*, *146*(6), 04020007. https://doi.org/10.1061/(ASCE)IR.1943-4774.0001464

Huete, A. R. (1988). A soil-adjusted vegetation index (SAVI). *Remote Sensing of Environment*, *25*(3), 295–309.

Ian R. McCann & Jeffery C. Stark. (1991). *Method and apparatus for variable application of irrigation water and chemicals* (Patent No. 5,246,164).

Ines, A. V. M., & Honda, K. (2005). On quantifying agricultural and water management practices from low spatial resolution RS data using genetic algorithms: A numerical study for mixed-pixel environment. *Advances in Water Resources*, *28*(8), 856–870. https://doi.org/10.1016/j.advwatres.2004.11.015

Jackson, R. D., Idso, S. B., Reginato, R. J., & Pinter Jr., P. J. (1981). Canopy temperature as a crop water

stress indicator. *Water Resources Research*, *17*(4), 1133–1138. https://doi.org/10.1029/WR017i004p01133

Kamble, B., Kilic, A., & Hubbard, K. (2013). Estimating crop coefficients using remote sensing-based vegetation index. *Remote Sensing*, 5(4), 1588–1602. https://doi.org/10.3390/rs5041588

Karthikeyan, L., Chawla, I., & Mishra, A. K. (2020). A review of remote sensing applications in agriculture for food security: Crop growth and yield, irrigation, and crop losses. *Journal of Hydrology*, *586*, 124905. https://doi.org/10.1016/j.jhydrol.2020.124905

Kranz, Evans, Lamm, O□Shaughnessy, & Peters. (2012). A Review of Mechanical Move Sprinkler Irrigation Control and Automation Technologies. *Applied Engineering in Agriculture*, *28*(3), 389–397. https://doi.org/10.13031/2013.41494

Lamm, D. F. R., & Porter, D. D. O. (2017). Ogallala Aquifer Program Center Pivot Irrigation Technology Transfer Effort. *Ogallala Aquifer Program Center Pivot Irrigation Technology Transfer Effort*. Irrigation Association Technical Conference, Orlando, FL.

Land and Water Division. (2002). *Deficit irrigation practices*. FAO. https://www.fao.org/publications/card/en/c/0504e958-62cf-5a86-93fb-2ca5e2906bb0/

Lo, T. H., Heeren, D. M., Mateos, L., Luck, J. D., Martin, D. L., Miller, K. A., Barker, J. B., & Shaver, T. M. (2017). Field Characterization of Field Capacity and Root Zone Available Water Capacity for Variable Rate Irrigation. *Applied Engineering in Agriculture*, *33*(4), 559–572. https://doi.org/10.13031/aea.11963

Li, W., Niu, Z., Chen, H., Li, D., Wu, M., & Zhao, W. (2016). Remote estimation of canopy height and aboveground biomass of maize using high-resolution stereo images from a low-cost unmanned aerial vehicle system. *Ecological Indicators*, 67, 637–648. https://doi.org/10.1016/j.ecolind.2016.03.036

Liakos, V., Vellidis, G., Tucker, M., Lowrance, C., & Liang, X. (2015). A decision support tool for managing precision irrigation with center pivots. *In J. V. Stafford (Ed.), Precision agriculture '15* (pp. 677 684). Wageningen Academic Publishers. https://doi.org/10.3920/978-90-8686-814-8_84

Maes, W. H., & Steppe, K. (2019). Perspectives for Remote Sensing with Unmanned Aerial Vehicles in Precision Agriculture. *Trends in Plant Science*, *24*(2), 152–164.

https://doi.org/10.1016/j.tplants.2018.11.007

Mahan, J. R., Conaty, W., Neilsen, J., Payton, P., & Cox, S. B. (2010). Field performance in agricultural settings of a wireless temperature monitoring system based on a low-cost infrared sensor. *Computers and Electronics in Agriculture*, 71(2), 176–181. https://doi.org/10.1016/j.compag.2010.01.005

Marshall, E., Aillery, M., Malcolm, S., & Williams, R. (2015). Agricultural Production under Climate Change: The Potential Impacts of Shifting Regional Water Balances in the United States. *American Journal of Agricultural Economics*, *97*(2), 568–588. https://doi.org/10.1093/ajae/aau122

McGuire, V. L. (2017). Water-level and recoverable water in storage changes, High Plains aquifer, predevelopment to 2015 and 2013–15. In *Water-level and recoverable water in storage changes, High Plains aquifer, predevelopment to 2015 and 2013–15* (USGS Numbered Series No. 2017–5040; Scientific Investigations Report, Vols. 2017–5040, p. 24). U.S. Geological Survey. https://doi.org/10.3133/sir20175040

Moran, M.S. & Clarke, T.R. & Inoue, Y. & Vidal, A.. (1994). Estimating crop water deficit using the relation between surface-air temperature and spectral vegetation index. *Remote Sensing of Environment.* 49. 246-263. 10.1016/0034-4257(94)90020-5.

Mudede, M. F., Newete, S. W., Abutaleb, K., & Nkongolo, N. (2020). Monitoring the urban environment quality in the city of Johannesburg using remote sensing data. *Journal of African Earth Sciences*, 171, 103969. https://doi.org/10.1016/j.jafrearsci.2020.103969

Mukherjee, A., Misra, S., & Raghuwanshi, N. S. (2019). A survey of unmanned aerial sensing solutions in precision agriculture. *Journal of Network and Computer Applications*, *148*, 102461. https://doi.org/10.1016/j.jnca.2019.102461

Myneni, R. B., Ramakrishna, R., Nemani, R., & Running, S. W. (1997). Estimation of global leaf area index and absorbed PAR using radiative transfer models. *IEEE Transactions on Geoscience and Remote Sensing*, *35*(6), 1380–1393.

Neale, Bausch, & Dale F. Heermann. (1989). Development of reflectance-based crop coefficients for corn.

Transactions of the ASAE, 32(6), 1891. https://doi.org/10.13031/2013.31240

NeSmith, D. s., & Ritchie, J. t. (1992). Short- and long-term responses of corn to a pre-anthesis soil water deficit. *Agronomy Journal*, 84(1), 107–113. https://doi.org/10.2134/agronj1992.00021962008400010021x

O'Shaughnessy, S. A., & Evett, S. R. (2008). Integration of wireless sensor networks into moving irrigation systems for automatic irrigation scheduling. 21.

O'Shaughnessy, S.A. & Evett, S.R. (2010). Developing wireless sensor networks for monitoring crop canopy temperature using a moving sprinkler system as a platform. *Applied Engineering in Agriculture*, 26(2), 331–341. https://doi.org/10.13031/2013.29534

O'Shaughnessy, S. A., Evett, S. R., Andrade, M. A., Workneh, F., Price, J. A., & Rush, C. M. (2016). Site specific variable-rate irrigation as a means to enhance water use efficiency. *Transactions of the ASABE*, 59(1), 239–249. https://doi.org/10.13031/trans.59.11165 Pfeiffer, L., & Lin, C.-Y. C. (2010). The effect of irrigation technology on groundwater use. *Choices*, 25(3). JSTOR. https://www.jstor.org/stable/choices.25.3.05

Perry, C.A., 2006, Effects of irrigation practices on water use in the Groundwater Management Districts within the Kansas High Plains, 1991-2003: U.S. Geological Survey Scientific Investigations Report 2006-5069, 93 p.

Pfeiffer, L., & Lin, C.-Y. C. (2014). Does efficient irrigation technology lead to reduced groundwater extraction? Empirical evidence. *Journal of Environmental Economics and Management*, 67(2), 189–208. https://doi.org/10.1016/j.jeem.2013.12.002

Pinter, Jr., P. J., Hatfield, J. L., Schepers, J. S., Barnes, E. M., Moran, M. S., Daughtry, C. S. T., & Upchurch, D. R. (2003). Remote Sensing for Crop Management. *Photogrammetric Engineering & Remote Sensing*, *69*(6), 647–664. https://doi.org/10.14358/PERS.69.6.647

Pôças, I., Calera, A., Campos, I., & Cunha, M. (2020). Remote sensing for estimating and mapping single and basal crop coefficients: A review on spectral vegetation indices approaches. *Agricultural Water*

Management, 233, 106081. https://doi.org/10.1016/j.agwat.2020.106081

Porter, D. O., Irmak, S., Lamm, F., Marek, T., & Rein, B. (2020). Challenges and Opportunities for Education in Irrigation Engineering. *Transactions of the ASABE*, *63*(5), 1289–1294. https://doi.org/10.13031/trans.13943

Rouse, J. W., Haas, R. H., Schell, J. A., Deering, D. W., & others. (1974). Monitoring vegetation systems in the Great Plains with ERTS. *NASA Special Publication*, *351*(1974), 309.

Rudd, J. D., Roberson, G. T., & Classen, J. J. (2017). Application of satellite, unmanned aircraft system, and ground-based sensor data for precision agriculture: A review. *2017 Spokane, Washington July 16 - July 19, 2017*. 2017 Spokane, Washington July 16 - July 19, 2017. https://doi.org/10.13031/aim.201700272

Sammis, C. L. Mapel, D. G. Lugg, R. R. Lansford, & J. T. McGuckin. (1985). Evapotranspiration crop coefficients predicted using growing-degree-days. *Transactions of the ASABE*, 28(3), 773–780. https://doi.org/10.13031/2013.32336

Sanderson, M. R., & Frey, R. S. (2015). Structural impediments to sustainable groundwater management in the High Plains Aquifer of western Kansas. *Agriculture and Human Values*, *32*(3), 401–417. https://doi.org/10.1007/s10460-014-9567-6

Scanlon, B. R., Faunt, C. C., Longuevergne, L., Reedy, R. C., Alley, W. M., McGuire, V. L., & McMahon, P. B. (2012). Groundwater depletion and sustainability of irrigation in the US High Plains and Central Valley. *Proceedings of the National Academy of Sciences*, *109*(24), 9320–9325. https://doi.org/10.1073/pnas.1200311109

Senay, G. B., Friedrichs, M., Singh, R. K., & Velpuri, N. M. (2016). Evaluating Landsat 8 evapotranspiration for water use mapping in the Colorado River Basin. *Remote Sensing of Environment*, 185, 171–185. https://doi.org/10.1016/j.rse.2015.12.043

Senay, G. B., Schauer, M., Friedrichs, M., Velpuri, N. M., & Singh, R. K. (2017). Satellite-based water use dynamics using historical Landsat data (1984–2014) in the Southwestern United States. *Remote Sensing of Environment*, 202, 98–112. https://doi.org/10.1016/j.rse.2017.05.005

Serrano, J., Shahidian, S., Marques da Silva, J., Paixão, L., Moral, F., Carmona-Cabezas, R., Garcia, S., Palha, J., & Noéme, J. (2020). Mapping Management Zones Based on Soil Apparent Electrical Conductivity and Remote Sensing for Implementation of Variable Rate Irrigation—Case Study of Corn under a Center Pivot. *Water*, *12*(12), 3427. https://doi.org/10.3390/w12123427

Sheffield, L. F. (1970). *The Impact of Center Pivot Irrigation in Southwest Nebraska* (No. 1723 2016-140165).

Shi, X., Han, W., Zhao, T., & Tang, J. (2019). Decision support system for variable rate irrigation based on UAV multispectral remote sensing. *Sensors*, 19(13), 2880. https://doi.org/10.3390/s19132880

Singh, R. K., Senay, G. B., Velpuri, N. M., Bohms, S., Scott, R. L., & Verdin, J. P. (2014). Actual evapotranspiration (water use) assessment of the Colorado River Basin at the Landsat resolution using the Operational Simplified Surface Energy Balance Model. *Remote Sensing*, 6(1), 233–256. https://doi.org/10.3390/rs6010233

Sishodia, R. P., Ray, R. L., & Singh, S. K. (2020). Applications of Remote Sensing in Precision Agriculture: A Review. *Remote Sensing*, *12*(19), 3136. https://doi.org/10.3390/rs12193136

Smidt, S. J., Haacker, E. M. K., Kendall, A. D., Deines, J. M., Pei, L., Cotterman, K. A., Li, H., … Hyndman, D. W. (2016). Complex water management in modern agriculture: Trends in the water-energy-food nexus over the High Plains Aquifer. *Science of The Total Environment*, 566–567, 988–1001. https://doi.org/10.1016/j.scitotenv.2016.05.127

Sophocleous, M. (2012). The evolution of groundwater management paradigms in Kansas and possible new steps towards water sustainability. Journal of Hydrology, 414–415, 550–559. https://doi.org/10.1016/j.jhydrol.2011.11.002

Stone, K. C., Bauer, P. J., O'Shaughnessy, S., Andrade-Rodriguez, A., & Evett, S. (2020). A variable-rate irrigation decision support system for corn in the U.S. Eastern Coastal Plain. *Transactions of the ASABE*, 63(5), 1295–1303. https://doi.org/10.13031/trans.13965

Sui, R., O'Shaughnessy, S. A., Evett, S. R., Andrade-Rodriguez, A., & Baggard, J. (2020). Evaluation of a

Decision Support System for Variable-Rate Irrigation in a Humid Region. *Transactions of the ASABE*, *63*(5), 1207–1215. https://doi.org/10.13031/trans.13904

Svedin, J. D., Kerry, R., Hansen, N. C., & Hopkins, B. G. (2021). Identifying Within-Field Spatial and Temporal Crop Water Stress to Conserve Irrigation Resources with Variable-Rate Irrigation. *Agronomy*, *11*(7), 1377. https://doi.org/10.3390/agronomy11071377

Szewczak, K., Łoś, H., Pudełko, R., Doroszewski, A., Gluba, Ł., Łukowski, M., Rafalska-Przysucha, A., … Usowicz, B. (2020). Agricultural drought monitoring by MODIS potential evapotranspiration remote sensing data application. *Remote Sensing*, 12(20), 3411. https://doi.org/10.3390/rs12203411

Talsma, C. J., Good, S. P., Jimenez, C., Martens, B., Fisher, J. B., Miralles, D. G., McCabe, M. F., & Purdy, A. J. (2018). Partitioning of evapotranspiration in remote sensing-based models. *Agricultural and Forest Meteorology*, *260–261*, 131–143. https://doi.org/10.1016/j.agrformet.2018.05.010

Thorp, K. R., & Bronson, K. F. (2013). A model-independent open-source geospatial tool for managing point-based environmental model simulations at multiple spatial locations. *Environmental Modelling & Software*, 50, 25–36. https://doi.org/10.1016/j.envsoft.2013.09.002

Tidwell, V., Vargas, V., Jones, S., Dealy, B., Shaneyfelt, C., Smith, B., & Moreland, B. (2016). *Analysis of High Plains Resource Risk and Economic Impacts* (No. SAND2016-3405, 1248575, 638112; pp. SAND2016-3405, 1248575, 638112). https://doi.org/10.2172/1248575

Tilman, D., Balzer, C., Hill, J., & Befort, B. L. (2011). Global food demand and the sustainable intensification of agriculture. *Proceedings of the National Academy of Sciences*, *108*(50), 20260–20264. https://doi.org/10.1073/pnas.1116437108

van der Merwe, D., Burchfield, D. R., Witt, T. D., Price, K. P., & Sharda, A. (2020). Chapter One—drones in agriculture. In D. L. Sparks (Ed.), *Advances in Agronomy* (Vol. 162, pp. 1–30). Academic Press. https://doi.org/10.1016/bs.agron.2020.03.001

Wada, Y., Wisser, D., Eisner, S., Flörke, M., Gerten, D., Haddeland, I., Hanasaki, N., Masaki, Y., Portmann, F. T., Stacke, T., Tessler, Z., & Schewe, J. (2013). Multimodel projections and uncertainties of irrigation

water demand under climate change. *Geophysical Research Letters*, *40*(17), 4626–4632. https://doi.org/10.1002/grl.50686

White, S. E. (1994). Ogallala Oases: Water Use, Population Redistribution, and Policy Implications in the High Plains of Western Kansas, 1980-1990. *Annals of the Association of American Geographers*, *84*(1), 29–45.

Zhang, J., Guan, K., Peng, B., Jiang, C., Wang, Z., Yang, Y., . . . Cai, Y. (2021). Challenges and opportunities in precision irrigation decision-support systems for center pivots. *Environmental Research Letters*, *16*(5). http://dx.doi.org.er.lib.k-state.edu/10.1088/1748-9326/abe436

Zhang, K., Kimball, J. S., & Running, S. W. (2016). A review of remote sensing based actualevapotranspiration estimation. *WIREs Water*, *3*(6), 834–853. https://doi.org/10.1002/wat2.1168